AN ABSTRACT OF THE DISSERTATION OF

James R. Keller for the degree of Doctor of Philosophy in Medical Physics presented on June 3, 2013.

Title: Extending the Clinical Applications of Commercially Available Optically Stimulated Luminescence (OSL) Dosimeters

Abstract approved: _____

Wolfram Laub

We present the results of our experiments designed to extend the clinical applications of commercially available Optically Stimulated Luminescence (OSL) Dosimeters. Our initial experiments demonstrate the linear response of the OSL dosimeters for doses under 200 cGy and the non-linear response of the device after 200 cGy. Our experiments show the signal depletion due to the reading out of commercial OSL dosimeters is 0.05%. Extending a calibration curve beyond the range of dose measurements used to derive the curve can lead to an error in measurements greater than 10%. Our method of optically bleaching the dosimeters with a light box housing 15 W compact fluorescence lamps reduces the accumulative dose on the dosimeters by 38% of the initial dose every time the bleaching time is doubled after 10 minutes.

The plausibility of the repeated use of OSL dosimeters with and without optically bleaching the devices is called into question based on the precision and accuracy seen

in our next experiments. The reliability of dose measurements varies depending on whether 6 MV, 10 MV, or 18 MV photons were used to repeatedly irradiate the OSL dosimeters. However, the uncertainty in all measurements where the devices were optically bleached remains less than 2% throughout our experiment. In contrast, the uncertainty in repeated measurements for commercial OSL dosimeters when the devices were not optically bleached display an increasing uncertainty quickly surpassing 5% as increasing amounts of dose accumulates on the device.

Through integration of the OSL dosimeter with the INTRABEAM™ system, we have developed a quality assurance procedure that tests deviation of the soft x-ray ionization chamber used with the system. The test can detect a deviation in an ionization chamber reading of 3.5% for the 50 kVp setting and 4.5% at the 40 kVp INTRABEAM™ setting. The OSL dosimeters are also used to determine the dose fall off of the output attenuated by a solid water phantom of varying thickness. An exponentially decreasing curve fits the dose measurements.

Extending the Clinical Applications of Commercially Available Optically Stimulated Luminescence (OSL) Dosimeters

by

James R. Keller

A DISSERTATION

submitted to

Oregon State University

in partial fulfillment of
the requirements for the
degree of

Doctor of Philosophy

Presented June 3, 2013
Commencement June 2014

Doctor of Philosophy dissertation of James R. Keller presented on June 3, 2013.

APPROVED:

Major Professor, representing Medical Physics

Head of the Department of Nuclear Engineering and Radiation Health Physics

---

Dean of the Graduate School

I understand that my dissertation will become part of the permanent collection of Oregon State University libraries. My signature below authorizes release of my dissertation to any reader upon request.

James R. Keller, Author

ACKNOWLEDGEMENTS

Academic

I want to thank Dr. Camille Palmer for her kindness and understanding throughout this whole ordeal. Thank you for introducing me to this field and your support in finishing this degree.

Without a doubt, I am truly in debt to Dr. William Hetherington. His kindness throughout my entire time at Oregon State University is unparalleled. I cannot say enough of his wisdom to know when to be a teacher, an instructor, a mentor, and a friend.

I'd also like to take this opportunity to express my gratitude to the Lee and Connie Kearney scholarship foundation, the Theron M. Bradley, Jr. Scholarship Foundation, the Department of Nuclear Engineering and Radiation Health Physics at Oregon State University, and the Department of Oncology at Oregon Health & Science University. Without their collective funding, this body of work would not have been completed.

Personal

I wish to thank my family for their continued support throughout my life and especially through this process. It takes good times and bad times to mold a person and only my family has been there for it all. Mom, Dad, Regina, Michael, Ethan, and Brett, thank you. You've done more than you know.

I'd also like to think my fellow graduate students in the Physics and NE/RHP depart-

ments at Oregon State University for taking me seriously and not so seriously. Thank you for your encouragement and inspiration. A special thanks goes to Alex and Mike who I've shared an office with this last year for making me laugh and remembering every silver lining has got a touch of grey.

TABLE OF CONTENTS

TABLE OF CONTENTS (Continued)

TABLE OF CONTENTS (Continued)

LIST OF FIGURES

LIST OF FIGURES (Continued)

LIST OF TABLES

Extending the Clinical Applications of Commercially Available Optically Stimulated Luminescence (OSL) Dosimeters

1 Introduction

1.1 Statement of the Problem

Delivery systems for radiation therapy treatments continue to improve demanding greater precision for devices that test the quality of treatments. In the past, the choice for a passive dosimeter has fallen on the thermoluminescence (TL) dosimeter which can be used for *in vivo* dosimetry and quality assurance of radiation therapy delivery systems (Kirby *et al.*, 1986). Even though TL dosimeters have been shown to have low relative error (Kirby *et al.*, 1992) and are well characterized, interest in new types of dosimeters is on the rise because of the shortcomings of TL dosimeters usage namely, careful heating techniques, energy dependence, and the loss of all information after the read out process.

Optically stimulated luminescence (OSL) dosimeters are an example of an advancement in passive dosimeter devices which addresses some of the TL dosimeter issues. The problem with OSL dosimeters is their relative recent introduction in the medical field. Where TL dosimeters have many years of laboratory and clinic characterization, OSL dosimeters have quite a few less years devoted to their characterization. And, the literature has not been so forthcoming with methods beyond pure observation that provide action toward proper clinical techniques.

The aim of this study is to bring to light techniques that can be incorporated in a

clinical setting to provide better use of the commercially available OSL dosimeter. In order to understand the behavior of the OSL dosimeter, this study begins by looking at the dose response of the devices and the effect of the reading out procedure. The main focus of this study centers on the repeatability of dose measurement for optically bleached dosimeters and comparing the output to non-bleached OSL dosimeters with the goal of creating techniques necessary to accomplish accurate measurements. Finally, the OSL dosimeters are used with a new type of radiation delivery system as an application to show the versatility and potential of the dosimeters.

1.2 Organization of this Thesis

This thesis contains six distinct chapters. The introduction being the first of the chapters incorporates basic ideas of how radiation interacts with matter, how certain materials will change due to radiation interactions, then how certain materials are reverted back to their initial state through luminescence. The future considerations, which is the final chapter, outlines the direction that could be considered for future experiments. Future considerations consist of improvements on existing experiments and new applications for the optically stimulated luminescence dosimeters.

Each of our experiments is outlined in the theory and background, methods, results, and conclusion chapters. Each chapter, like the theory and background chapter, contains all the theory and background information for all the experiments. Likewise, the method chapter contains all the methods for each of our experiments.

2 Theoretical and Material Background

Chapter 2 outlines the basic ideas for how radiation and solid state detectors interact. It begins with an introduction to the types of interactions of radiation and the luminescence process of materials. Next, the material properties of Aluminum Oxide (Al_2O_3) are included along with changes due to introducing a carbon doping material to the crystal. Finally, chapter 2 contains the clinical relevance of the behavior of Aluminum Oxide doped with Carbon.

2.1 Introduction to Basic Radiation Interactions

Before a meaningful discussion of measuring dose or how devices interact with radiation can begin, it is necessary to introduce the ideas of how matter and radiation interact. So, to begin, a basic introduction to radiation and its interaction with mater is included below.

As a general classification, radiation interactions with matter can be divided into either ionizing or non-ionizing. Even though non-ionizing radiation offers a plethora of matter interaction phenomena to study, this study focuses on the interaction of matter with ionizing radiation.

Ionizing radiation consists of electromagnetic waves and subatomic particles that have enough energy to excite or ionize atoms and molecules. Energy necessary to ion-

ize an atom or molecule varies but typical values are between 4 and 25 eV (Attics, 1986). The types of particles that can deliver ionizing radiation can vary amongst charged particles and uncharged particles; however, this study is only concerned with photon and electron particle interactions.

The photon interaction is considered an indirect ionizing radiation because the photon imparts its energy to the material medium producing charged particles. And, these newly liberated charged particles then continue to ionize the material through Coulomb interactions. The three types of photon interactions that are important to radiation detection are the photoelectric effect, Compton Scattering, and pair production (Tsoulfanidis, 1995, Knoll 2010, Kahn 2010).

The photoelectric effect occurs when a photon is absorbed by an electron bounded by an atom within the medium of the photons propagation. The energy of the photon, E_γ, is given in EQ.(2.1), where ν is the frequency of the photon and h is Plank's constant. If the energy of the interacting photon is greater than the binding energy, B_e, the electron in ionized from the atom with kinetic energy, K_e, given in EQ.(2.2). As an approximation, the energy of the photon is considered much greater than the binding energy of the electron. Thus, the kinetic energy of the ionized electron is approximately the energy of the interacting photon.

$$E_\gamma = h\nu \tag{2.1}$$

$$K_e = E_\gamma - B_e \tag{2.2}$$

The microscopic cross section can be thought of as the interaction probability per unit differential path length, normalized to one target atom per unit volume (Shultis and Faw, 2002). The microscopic cross section is directly proportional to the attenuation coefficient, which is the probability of interaction for a given path length. The linear attenuation coefficient for the photoelectric effect, μ_{pe}, is proportional to the photon energy, E_γ, and the density of the material, Z, shown in EQ.(2.3) (Turner, 2010). It should be noted that the Z dependence of μ_{pe} is a rough approximation and has values of about 4 for photon energies of 100 keV and 4.6 for 3 MeV (Shultis and Faw, 2002). The proportionality of the attenuation coefficient illustrates that the photoelectric interactions have a high probability of occurring when photons of low energy interact with high density materials.

$$\mu_{pe} \propto \sigma_{pe} \propto \frac{Z^4}{E_\gamma^3} \tag{2.3}$$

Compton Scattering occurs at greater incident photon energies. When this method of interaction occurs, the photon does not impart its entire energy to the electron. Thus, after the interaction, the resulting products are a liberated electron, a photon with less energy than the incident photon, and an ionized atom. The exiting photon energy, which is shown in EQ.(2.4), can be derived from the conservation of momentum and energy comparing the before and after states of the system given the incident photon energy, E_γ, the scattering angle of the exiting photon, θ_{sc}, and the mass of the electron, $m_e c^2 = 0.511 MeV$ (Tsoulfanidis, 1995, Knoll 2010, Kahn 2010). The kinetic energy of the electron, k_e can be determined with EQ.(2.5) given the incident photon energy, E_γ, the

exiting photon energy, E'_γ, and the binding energy, B_e.

$$E'_\gamma = \frac{E_\gamma}{1 + \frac{E_\gamma}{m_e c^2}(1 - \cos\theta_{sc})} \tag{2.4}$$

$$K_e = E_\gamma - B_e - E'_\gamma \tag{2.5}$$

Compton Scattering can be investigated in the two extreme scattering angles equating to a head on collision between the photon and electron and at the grazing angle where the photon and electron have a minimal interaction. These two case studies show the energy detected from Compton Scattering is dependent on the scattering angle.

A head on collision between the photon and electron translates to a scattering angle of 180° meaning the exiting photon is propagated in the opposite direction as its incident direction. When the scattering angle is 180°, the exiting photon is given by EQ.(2.6). The corresponding electron kinetic energy is given in EQ.(2.7) using EQ.(2.5) and assuming the binding energy is negligible compared to the total incident photon energy.

$$E'_\gamma = \frac{E_\gamma}{1 + 2\frac{E_\gamma}{m_e c^2}} \tag{2.6}$$

$$K_e = \frac{E_\gamma}{1 + \frac{m_e c^2}{2E_\gamma}} \tag{2.7}$$

At the grazing angle, the scattering angle is equal to 0°. In this case, the exiting photon energy is equivalent to the incident photon energy and the kinetic energy of the exiting electron is approximately zero.

The Compton Scattering attenuation coefficient, μ_{cs} has a different proportionality dependence compared to the photoelectric effect. For Compton Scattering, μ_{cs} is given in EQ(2.8), where N is the atomic density given by EQ(2.9) and N_A is Avogadro's number and A is the atomic mass number.

$$\mu_{cs} \propto NEZ \tag{2.8}$$

$$N = \rho \frac{N_A}{A} \tag{2.9}$$

As an approximation, the atomic mass number A can considered equivalent to $2Z$, two times the atomic number. This approximation allows EQ.(2.8) to be rewritten as EQ.(2.10) showing the only dependence of μ_{cs} is on the density of the material and the energy of the incident photon.

$$\mu_{cs} \propto \rho \frac{N_A}{2} E_\gamma \tag{2.10}$$

Pair production is the final photon interaction process discussed in this introduction. The interaction process occurs in the presence of the strong nuclear field surrounding the nucleus and has a threshold energy of $2m_e c^2$ which is 1.022 MeV (Shultis, 2002). Upon the process occurrence, the incident photon is absorbed and an electron-positron pair appears. The kinetic energy of the final particles is determined with EQ(2.11) where K_{e^-} and K_{e^+} are the final kinetic energy of the electron and position, respectively (Shultis, 2002).

$$K_{e^-} + K_{e^+} = E_\gamma - 2m_e c^2 \tag{2.11}$$

Once created, the electron and positron continue to interact with the surrounding medium. The positron faces annihilation once its kinetic energy approaches zero through its numerous interaction and then easily recombines with an electron. Two photons of energy $m_e c^2$ are then created upon annihilation (Tsoulfanidis, 1995, Shultis and Faw, 2002, Knoll 2010, Kahn 2010).

As a final note, the total probability of a photon interacting with a given material is the summation of each of the probabilities from the individual contributing interactions. This summation is known as the total attenuation coefficient (Shultis, 2002). Often reported is the total mass interaction coefficient, which is the total attenuation coefficient divided by the density of the material.

2.2 Introduction to Luminescence Models

To begin the discussion about luminescent models, we should start with the general classification of materials, namely conductors, semiconductors, and insulators. The categorical difference between these types of materials depends on their ability to conduct an electric field. Looking at the energy bands of the materials, conductors have overlapping conduction and valance energy bands while bands in insulators and semi-conductors are separated(S.L. Kakani and A. Kakani, 2004),which produces a band gap. Insulators are marked by a large band gap while semi-conductors are not as large and their ability to conduct changes with temperature (S.L. Kakani and A. Kakani, 2004).

For an electron in the valance band of an insulator, an external source can supply the electron enough energy to excite it through the band gap to the conduction band leaving a “hole” in its place (Ashcroft and Mermin, 1979). The “hole” is an abstraction representing the absence of an electron in the sea of electrons in the valance band and can be thought of as having a positive charge. Once in the conduction band, the electron is free to return to the ground state and recombine with the “hole” by either radiative or non-radiative means (Attix, 1986). For this study, the external source for exciting electrons will consist of ionizing radiation and the radiative process is only interesting form of de-excitation, since this process produces luminescence.

The introduction of impurities during the crystal formation process creates energy levels within the band gap of a pure crystal and the new energy levels become trapping centers for charge carriers in the crystal. The defects within the crystal as a results of the impurities are regions of the pure crystal where there are an excess or a deficit of ions. These local regions of charge excess or deficit locally attract charge carriers. Once a charge carrier is bound to one of these defect regions the charge carrier is considered trapped because additional energy is required to release the electron from its bondage.

The transition of charge carriers between energy levels in the conduction band and valence band as well as defective energy levels and the eventual recombination is the essential behavior producing luminescence. Upon the absorption of ionizing radiation, the electron is excited to the conduction band leaving a “hole” in the valence band. Both charge carriers then migrate to local defective charge regions in the band gap - the electron to ion deficient regions and the “hole” to ion surplus regions. Once in a defective region, the electron is considered trapped. External stimulation can excite the

electron out of the trap and back to the conduction band. At this point, the electron can de-excite to one of the deficit "hole" sites and recombine which releases photons detected as luminescences (McKeever, 1985, Jursinic, 2007).

2.2.1 One Trap Model

The simplest model for luminescence within in a crystal models one electron trap and one "hole" trap (Botter-Jensen et al., 2003). This single trap and center model assumes emission occurs when the excited electron recombines with a hole and that there is only one pathway for the electron which results in recombination with the hole.

The charge concentration in each of the traps changes as the electrons receive stimulation that frees them from their traps. If n is the concentration of trapped electrons, n_c the concentration of electrons in the conduction band, and m the concentration of hole traps, the rate of change for the charge concentrations is shown by EQ.(2.12).

$$\frac{dn_c}{dt} = -\frac{dn}{dt} + \frac{dm}{dt} \tag{2.12}$$

The rate of change for the trapped electrons and holes can individually be expressed with EQ.(2.13) and EQ.(2.14), respectively. The rate of stimulation is represented with p; the number of electron traps is N; the trapping probability is A; the recombination probability is A_m; and finally τ is the electron recombination time.

$$\frac{dn}{dt} = np - n_c A(N - n) \tag{2.13}$$

$$\frac{dm}{dt} = n_c A_m m = \frac{n_c}{\tau} \tag{2.14}$$

If the material is assumed to be in a quasi-equilibrium state meaning the concentration of electrons in the conduction band does not change very much compared to the concentration change of the electron traps and hole traps then EQ.(2.12) reduces to EQ.(2.15) (Vij, 1998).

$$\frac{dn}{dt} = \frac{dm}{dt} \tag{2.15}$$

If the assumption that the re-trapping of electrons is minute compared to the stimulation process applies (i.e. $n_c A(N-n) \ll np$), the intensity of the luminescence signal is expressed with EQ.(2.16) (Vij, 1998). In this simplified model, the intensity of the luminescence signal is directly proportional to the rate of stimulation.

$$I = -\frac{dn}{dt} = np \tag{2.16}$$

Solving EQ.(2.16) for the concentration of trapped electrons, n, and then multiplying by the stimulation rate, p, the intensity of the luminescence in terms of the stimulation time is obtained, which is shown in EQ.(2.17), where the lifetime of the luminescences is $\tau = 1/p$. Therefore, under stimulation conditions, the single trap model says the luminescences is expected to decrease at an exponential rate.

$$I = I_0 \exp(-t/\tau) \tag{2.17}$$

2.2.2 Complex Model

The simple model with its assumptions demonstrates how the intensity of luminescence is directly proportional to the intensity of stimulating radiation. However, a more complex model is necessary to accurately model the true behavior for actual materials. The most complex model needs to introduce multiple types of levels along with including the many different pathways that exists for electrons after the absorption of ionizing radiation.

If the simple model is considered to describe the behavior of the main dosimetric traps, two other types of general traps are present in a more complicated model, namely the deep and shallow traps. Both of these traps are named because of the energy requirement necessary to return trapped electrons in these local defect regions to the conduction band.

The energy required to free electrons in shallow traps can be supplied by by thermal fluctuations at room temperature (Bøtter-Jensen *et al.*, 2003). Therefore, these traps are cleared soon after the initial electron occupation. Of course, luminescence can occur as recombination is a result of the stimulation of these traps, which results in a phosphorescence signal after irradiation (Yukihara and McKeever, 2008). The phosphorescence occurs for approximately 10 minutes after irradiation (Jursinic, 2007).

Once the shallow traps are cleared after 10 minute period of phosphorescence, they can then present themselves as a pathway for stimulated electrons from the dosimetric traps during read out. The charge competition then causes initial reading of dosimetric traps to be lower than expected (Yukihara and McKeever, 2008).

Deep traps also pose a possible pathway for excited electrons upon the absorption of ionizing radiation as the electrons settle into local deficit sites. And, upon stimulation of dosimetric trapped electrons to the conduction band, deep traps present a pathway for electrons to deep traps other than to recombination sites (Yukihara and McKeever, 2008). However, the deep traps are not directly stimulated, the occupancy of deep traps does not decrease making recombination for dosimetric electron stimulation more probable with the increase in dose history (Yukihara *et al.*, 2003, Yukihara and McKeever, 2008).

2.3 Material Properties

2.3.1 Aluminum Oxide

For this study, Aluminum Oxide is the crystal material of interest and is studied in its single crystal form (α-Al_2O_3). The physical properties include a density of 3.96 g/cm^3 and an effective atomic number of $Z_{eff} = 11.3$ (Johns and Cunningham, 1983). The crystal form of Aluminum Oxide, also known as Corundum, has a closed pack octahedral shape placing the metal ion at the corners surrounded by six oxygen atoms (Pauling and Hendricks, 1925).

The thermoluminescence properties of aluminum oxide were first explored by Rieke and Daniels, but the use of the material dosimetrically for its thermoluminescence properties was later shown not to be productive. However, adding carbon to the crystal enhances its optical luminescence properties for dosimetric use.

2.3.2 Aluminum Oxide Doped with Carbon

Aluminum Oxide doped with carbon (Al_2O_3:C) is manufactured by growing α-Al_2O_3 in a reducing atmosphere in the presence of carbon (Akselrod and Kortov, 1990; Akselrod *et al.*, 1990; Akselrod *et al.*, 1993). The addition of carbon impurities in the crystal structure increases the formation of oxygen vacancy centers which are the luminescence centers. The important luminescence centers can either accomedate one or two electrons and are referred to as *F-centers* or F^+*-centers*, respectively (Bøtter-Jensen et al., 2003.) The number of F^+*-centers* is directly proportional to the sensitivity of the crystal (McKeever *et al.*, 1999).

The luminescence process is believed to occur in Al_2O_3:C when an electron that has been excited to the conduction band is freed from a trapping center and recombines with a "hole" at an F^+-center. The F^+-center remains in an excited state for a lifetime of approximately 35 ms until it radiatively relaxes to an *F*-center (Akselrod *et al.*, 1998, Jursinic, 2007).

The recombination process results in an two emission bands centered at 420 nm and 330 nm (Akselrod *et al.*, 1990; Markey *et al.*, 1995). Where the 420 nm emission is associated with a recombination lifetime of 35 nm, the ultraviolet emission band has a lifetime of approximately 5 nm.

2.4 Determining Dose

For studies conducted with clinical relevance, it is necessary to relate a measure of irradiation to a measure of absorbed dose. In its most general definition, absorbed dose

is the mean energy imparted by ionizing radiation to a material of a certain mass (Kahn, 2010). The units for absorbed dose varies in usage across disciplines and the *rad* is the traditionally older unit relating 100 ergs of energy per gram of absorbing material. The common SI unit is the *gray* which is 1 J/kg, thus making 1 centigray (cGy) equal to 1 rad.

The dose to a medium can be determined from the dose to air which in turn can be related to the exposure to air. The exposure in air is given by EQ.(2.18), where Ψ_{air} is the photon energy flux, $(\bar{\mu}_{en}/\rho)$ is the mass energy absorption coefficient, and $\overline{W}$ is the the mean energy necessary to produce an ion pair in air, and e is the charge of the electron.

$$X = \Psi_{air}\left(\frac{\bar{\mu}_{en}}{\rho}\right)\left(\frac{e}{\overline{W}}\right) \tag{2.18}$$

The dose to air is the energy imparted to air per unit of mass and can be written as the photon energy flux, Ψ_{air}, times the mass energy attenuation,$(\bar{\mu}_{en}/\rho)$ shown in EQ.(2.19). With EQ.(2.18) and EQ.(2.19), the dose in air is related to the exposure by EQ.(2.20), where $\bar{W}$ has the typical and almost constant value of 33.97 eV/ion pair in dry air.

$$D_{air} = \frac{dE_{en}}{dm} = \Psi_{air}\left(\frac{\bar{\mu}_{en}}{\rho}\right) \tag{2.19}$$

$$D_{air} = X\frac{\overline{W}}{e} \tag{2.20}$$

The dose in any medium then becomes a ratio of the dose in the medium to the dose

in air as EQ.(2.21) shows. The exposure can be determined with a correctly calibrated ion chamber, with a calibration factor of N_x, and with M as the ion chamber measurement. Then, the dose in a medium can be written as in EQ.(2.22) with the assumption that the ion chamber is placed in the medium where electron charge equilibrium exists.

$$\frac{D_{med}}{D_{air}} = \frac{\Psi_{med}}{\Psi_{air}} \frac{(\bar{\mu}_{en}/\rho)_{med}}{(\bar{\mu}_{en}/\rho)_{air}} = \left.\frac{\bar{\mu}_{en}}{\rho}\right|_{air}^{med} \Psi_{air}^{med} \tag{2.21}$$

$$D_{med} = MN_x \frac{\overline{W}}{e} \left.\frac{\bar{\mu}_{en}}{\rho}\right|_{air}^{med} \Psi_{air}^{med} \tag{2.22}$$

2.4.1 Bragg-Gray Cavity Theory

Any method that relies on determining the exposure at the point of measurement to calculate the dose to a medium has limitations of only being useful for x-ray and γ-rays below 3 MeV. Also, electronic equilibrium must be established at the point of measurement (Kahn, 2010). The Bragg-Gray cavity theory is an alternative to calculating the dose to a medium that does not rely on the determinism of the exposure at the point of measurement.

The Bragg-Gray theory purposes a cavity at the point of measurement. This cavity is small enough that its introduction to the medium does not disturb the number of electrons exiting the cavity when the cavity is not present. If these conditions hold, the Bragg-Gray relationship for dose to a medium shown in EQ.(2.23) is satisfied. In EQ.(2.23), J_g is the ionization charge of a single sign ion per unit mass of the cavity and $\left(\bar{S}/\rho\right)_{air}^{med}$ is the mean ratio of stopping powers for electrons crossing the gas cavity to

the medium.

$$D_{med} = J_g \frac{\overline{W}}{e} \; \bar{S}/\rho \; {}^{med}_{g} \tag{2.23}$$

The stopping power is the energy loss by electrons per unit path length of the material (Kahn, 2010). The stopping power has been the focus of many studies and its usage in Bragg-Gray theory is the focus for accuracy improvements. One such improvement of on the theory is the Spencer-Attix cavity theory, which uses the restrictive mass collision stopping power in place of the mean stopping power.

The support of higher accuracy with the use of the restrictive mass collision stopping power is found in the assumption of the Bragg-Gray theory stating the cavity should not perturb the electron flux. As primary electrons and photons interact with the medium, secondary or δ-rays are created. Some of the δ-rays are low energy and are assumed to deposit their energy very close to their creation site. Therefore, upon entering the cavity, these low energy δ-rays will not transverse the cavity. These low energy δ-rays should not be considered in the calculation of dose to the medium. Thus, the restrictive mass collision stopping power excludes these low energy δ-rays by considering only electrons of a minimum energy (Attix, 1986).

2.4.2 Ion Chamber Measurements

Absorbed dose measurements can be determined from ion chamber measurements using the formalism of TG-51. The formalism of protocol TG-51 uses EQ.(2.24) to determine the absorbed dose in water from a beam of quality Q, where $N_{D,w}^{^{60}Co}$ is the absorbed

dose to water calibration factor for the ion chamber for a ^{60}Co beam under reference conditions and k_Q is the quality conversion factor for the chamber.

$$D_w^Q = M k_Q N_{D,w}^{^{60}Co} \tag{2.24}$$

The M term takes the raw reading from the ion chamber measurement, M_{raw} and corrects it with four different factors, as shown in EQ.(2.25). The four ion chamber correction factors correct for a discrepancies in ion recombination, P_{ion}, temperature and pressure differences from calibration conditions, $P_{T,P}$, any corrections necessary due electrometer, and ion chamber interactions, P_{elec}, and any correction needed for polarity.

$$M = M_{raw} P_{ion} P_{T,P} P_{elec} P_{pol} \tag{2.25}$$

Ion Recombination Factor, P_{ion}

The ion recombination factor corrects for two effects - saturation and collection efficiency (Kahn, 2010). The saturation effect is due to the functional behavior of the ion chamber where the response of the ion current is linear for low chamber voltages but then it becomes less responsive at higher voltages. Ideally, the ion chamber should be operated in the linear response region so small voltage variations do not result in large current changes.

The ion recombination correction factor is derived with EQ.(2.26), where two measurements are taken at a high and low voltage. For the high voltage measurement, M_{raw}^H is the electrometer reading in Coulombs and V_H is the voltage setting of the electrometer

and for the low voltage reading, M^L_{raw} is the measurement and V_L is the voltage setting.

$$P_{ion}(V_H) = \frac{1 - (V_H/V_L)^2}{M^H_{raw}/M^L_{raw} - (V_H/V_L)^2} \tag{2.26}$$

Temperature and Pressure Correction, $P_{T,P}$

According to the gas law relationship, in a fixed volume the amount of moles of a gas is directly proportional to the pressure and indirectly proportional to the temperature. So, a correction factor needs to be applied to a measurement to adjust for the any change in temperature and pressure at the time of measurement compared to the standard temperature and pressure, which is 22° Celsius and 1 atmosphere (101.33 kPa or 760 mmHg).

The temperature and pressure correction factor can be calculated with EQ.(2.27), where the temperature is in Celsius and the pressure is in kPa. A simple set of calculations reveals that a 3° increase in temperature increases $P_{T,P}$ by 1% and an 8 mmHg increase in pressure decreases the correction factor by 1%.

$$P_{TP} = \frac{273.2 + T}{273.2 + 22} \times \frac{101.33}{P} \tag{2.27}$$

Polarity Effect, P_{pol}

A correction factor is necessary when measuring the charge from an ion chamber if there is a difference in magnitude in charge when collecting charges of different polarity. This

effect can be the result of current collected outside of the sensitive region of the ion chamber for example by irradiation of electronic equipment.

The polarity effect correction can be determined by collecting the different charges over the course of two irradiations of the same magnitude. The correction factor is determined with EQ.(2.28), where the M^{+}_{raw} is the charge collected from positive ions, M^{-}_{raw} is the charge from the collection of negative ions, and M_{raw} is the charge collected from the same charge as used when the ion chamber is calibrated.

$$P_{pol} = \left| \frac{M^{+}_{raw} - M^{-}_{raw}}{2M_{raw}} \right| \tag{2.28}$$

Electrometer Correction Factor, P_{ion}

The electrometer correction factor is dependent on whether the ion chamber and electrometer are calibrated as a single unit of operation or considered separate. If they are considered separate, there needs to be a calibration factor to ensure the reading from the ion chamber accurately represents the amount of Coulombs collected. If they are one unit, the correction factor is simply 1.00.

2.5 Clinical Relevance

Commercially available aluminum oxide doped with carbon, Al_2O_3:C, has found a use in oncology departments in the United States for its dosimetric abilities. Their use has primarily been as a single use device where after some irradiation and a read out, the

devices have been discarded. However, the possibility for reuse exists because the devices are not destroyed during the irradiation process and may continue to function in a predictable manner.

In this section, we introduce the experimental methods for reducing accumulative dose on a commercial Al_2O_3:C device through optical bleaching. Also, we introduce the idea of reliability through reproducibility for the devices upon optical bleaching. Then, we discuss the idea of sensitivity changes that could occur as a result of optical bleaching. Finally, an application is discussed which illustrates the potential use of these devices.

2.5.1 Initial Experiments

The initial experiments comprise of a few experiments that are necessary to quantify the effects of reading out the dosimeters and establishing a calibration curve. Although these experiments are not considered novel, they state the current status of our devices and provide the foundation for future experiments.

Read Out Signal Depletion

The dosimeters require optical stimulation from the reader to induce luminescence. The photons from the luminescence are collected by a photomultipler tube and the current is reported as counts. As the dosimeter is readout intermediate traps are being cleared, thus the dose on the dosimeter is being reduced. Therefore, it is necessary to understand the depletion of signal that can be expected after a reading.

Dose Response

The nanoDot™ dosimeters have been shown to have two different regions of dose response (Yukihara *et al.*, 2004; Jursinic, 2007; Mrčela *et al.*, 2011). These two regions are marked by a linear region below 200 cGy and a non-linear response above 200 cGy. Authors have tried to model the two regions with a single curve (Jursinic, 2010). A piecewise model may provide the highest accuracy, but introduces a complexity of how to handle the cross over point.

Regardless of the complication of the cross over point, it is important to produce the dose response behavior reported in publications. An experiment designed to reproduce the dose response will give insight into the experimental set up and our handling of the dosimeters. This is a necessary set in establishing control over the dosimeter before moving forward.

Calibration Curve

A calibration curve provides the link between reading out the number of counts from an irradiated OSL dosimeter and the actual dose the dosimeter received. The generation of a calibration curve requires the irradiation of the OSL dosimeters over known dose amounts and then reading out the device to determine the number of counts for that dose point. The calibration curve in a general sense is the dose response for the material and the conversion of counts to dose is at the heart of all clinical measurements. The existence of the linear and non-linear dose response regions creates the necessity of two calibration curves, one for each of the respective response region.

2.5.2 Optical Bleaching within the Clinic

The optical bleaching of the commercially available optical stimulated luminescence (OSL) dosimeter is a method of reducing accumulative dose on the device. Different studies have compared the efficiency of reduction with the use of 14 W compact fluorescent lamps (CFL), 150 W tungsten-halogen lamps, and different wavelengths (Jursinic, 2007, Omotayo *et al.*, 2012).

The bleaching process is similar to the read out process where the active crystal region of the OSL dosimeter is exposed to optical light. However, where the read out process only lasts for a short duration of time and does not completely reduce the dosimetric traps, optical bleaching attempts to remove all the filled dosimetric traps. The read out process also uses a dedicated reader, which opens the dosimeter to expose the crystal region. The OSL dosimeter needs to be manually opened during the optical bleaching process.

The optical bleaching process does not clear out all trapped electrons within the material. The shallow traps, which are unstable at room temperature, receive enough stimulation from thermal fluctuations to free their trapped electrons. The exposure to optical light supplies enough stimulation only for dosimetic/intermediate trapped electrons. The deep traps remain filled during the optical bleaching process. Heating the material is necessary to supply stimulation to free deep trapped electrons (Yukihara *et al.*, 2003, Yukihara *et al.*, 2004). In general, the temperatures that are required would damage the housing of the commercial OSL dosimeters.

Although the ability to reduce the dose on an OSL dosimeter with optical light has

been shown by other authors, their methods are not easily reproduced within a clinical setting. We present a method that uses equipment found in a clinic without requiring specialized bleaching equipment.

2.5.3 Repeatability

In the clinical setting, nanoDot™ dosimeters are primarily a single use device, but there is interest in using these devices more than once as the applications continue to increase. One such application could be to measure skin dose for an external beam patient who receives radiation once a day for 5 to 7 weeks. If three to five nanoDot™ dosimeters are used for each fraction, the total number of dosimeters used is 15 to 35. The number of dosimeters increases for procedures like total body irradiations or total skin electron treatments.

The easiest way to reuse a nanoDot™ dosimeter is to know the initial dose before an irradiation and then determine the total dose after irradiation. The differences between the two doses would then constitute the dose for the irradiation. In this case, the dosimeter continues to accumulate dose during its entire usage. This method of use is actually how the dosimeter is used when it is only used once where the initial dose is assumed to be negligible.

The ability to optically bleach the nanoDot™ dosimeters provides another method for the reuse of the dosimeters. After the initial irradiation and readout, the dosimeters can be bleached until the accumulative dose is once again zero. This method allows the irradiation of dosimeters that always have a relatively small initial dose.

The goal of this experiment is to illustrate the precision and accuracy of repeated use of commercially available OSLDs within the clinical environment. Then using our bleaching technique, we compare the repeated use measurements of the nanoDot™ dosimeters between bleached dosimeters and non-bleached dosimeters. Finally, we look at the dose response in the linear region for nanoDot™ dosimeters with accumulative dose that have been optically bleached.

2.5.4 Sensitivity Changes

Sensitivity changes are expected for the nanoDot™ dosimeters with accumulative dose because of the subsequent filling of traps and the underlying statistical nature of charge trapping competition. A sensitivity change is also anticipated for a dosimeter after optical bleaching due to the fact that optical bleaching only stimulated and frees electrons in intermediate traps. Thus, less charge competition exists between deep and intermediate traps for a dosimeter after bleaching with partially filled deep traps than for a new dosimeter.

The necessity of understanding the sensitivity changes of nanoDot™ dosimeters stems from the desire to optically bleach the dosimeters for reuse in a clinical setting. If a proper calibration curve can be established based on the parameters that effect sensitivity, the calibration curve can be used for accurately determining the dose from the dosimeters.

The sensitivity (counts/Gy) has been reported as decreasing and the supra-linearity of the dosimeters as increasing for accumulative doses below 60 Gy (Jursinic, 2010). To

reiterate, dosimeters with an accumulative dose history below 60 Gy report more counts for a given amount of dose when read out.

The purpose of this experiment is to determine how the linear response region of the nanoDot™ dosimeters changes with accumulative dose. Specifically, this experiment attempts to determine new calibration curves for dosimeters with accumulative dose that have been optically bleached and are reused in a low dose irradiation situation.

2.5.5 INTRABEAM™ System

In previous decades, diagnosis of breast cancer usually resulted in a total mastectomy of the diseased breast. However, breast conserving surgery (BCS) has become a more prominent treatment due to its equivalent overall survival rates compared to mastectomy (van Dongen *et al.*,2000; Veronesi *et al.*, 2002; Fisher *et al.*, 2010). Coupling whole breast radiation therapy with BCS decreases the first reoccurrence by an absolute 15.7% compared to patients not receiving radiation therapy(E.B.C.T.C. Group, 2011). An additional dose of 10 to 16 Gy to the tumor bed after initial radiation therapy, known as a boost treatment, has been shown through randomized trials to further decrease the reoccurrence rate (Romestaing *et al.*, 1997; Bartelink *et al.*, 2001; Polgár *et al.*, 2002). Based upon these results, a modern external beam radiation treatment for breast cancer consists of BSC to remove the tumor followed by a five to six week external beam radiation therapy followed by a one to two week external beam boost treatment. Some patients may also receive chemotherapy because of their risk of systematic disease, which can add weeks of treatment that is usually administered prior to external radiation therapy.

Even though it is highly beneficial in reducing local relapse, whole breast irradiation with external beam radiation therapy (EBRT) has treatment disadvantages. With EBRT, the patient receives radiation to the whole breast which subjects them to side effects including desquamation, fibrosis, rib fragility, fibrosis of the lung, and fatigue. EBRT also has the disadvantage of requiring additional weeks to administer the prescribed dose causing some patients to refuse or not to complete the radiation portion of their treatment plan. Overcoming these disadvantages without compromising quality of care would increase the satisfaction and likelihood of completing the recommended treatment.

The Radiation Medicine department at OHSU has put itself in a very unique position to address the issues of EBRT as only one of 125 clinics in the world to offer radiation therapy to early stage breast cancer patients using the INTRABEAM™ system (Carl Zeiss, Oberkochen, Germany), which is shown in Fig. 2.1. The INTRABEAM™ system is a low energy x-ray source that administers a prescribed radiation dose in 20 to 50 minutes following the primary tumor lumpectomy in a procedure known as intraoperative radiation therapy (IORT) (Kraus-Tiefenbacher, 2005). This technique has been compared in a randomized controlled trial to whole breast irradiation given over 5 weeks, the TARGIT A trial. In this trial, 2232 patients were randomized to the two treatment arms and at 4 year follow up, there was no significant difference in the local recurrences of the two arms (1.2% for INTRABEAM™ and 0.95% whole breast). The conclusion of the study was that for selected patients with early breast cancer, a single dose of radiotherapy delivered at the time of surgery by use of targeted intraoperative radiotherapy should be considered as an alternative to external beam radiotherapy delivered over several weeks. (Vaidya *et al.*, 2010)

Figure 2.1: The INTRABEAM™ device allows positioning of the applicator into the BSC site of the patient after the primary tumor has been removed. The patient then receives a 20 to 30 minute radiation treatment delivered to the tumor bed. *www.meditec.zeiss.com/intrabeam*

Therefore, selection criteria for using this technique are critical to the success of the treatment. At OHSU, the patients who are eligible for treatment with INTRABEAM™ should meet the criteria set forth by the American Society for Radiation Oncology (ASTRO) for accelerated partial breast irradiation (APBI) (Smith *et al.*, 2010). The INTRABEAM™ as a treatment is considered by the ASTRO community to be an APBI treatment. Table(2.1) shows the ASTRO patient criteria.

The INTRABEAM™ device has the potential for treatment of cancer in other sites such as brain tumors, spine tumors, sarvomas, and potentially gastrointestinal tumors. As an example, for the first time in 2010, IORT with INTRABEAM™ was combined with kyphoplasty to provide stability, pain relief, and sterilization of metastasis in patients along the vertebral column (Wenz *et al.*, 2010).

The future use of IORT looks very promising, but the new procedures are not standard treatments and the few places that have the INTRABEAM™ system use it beyond

treatment for a small number of early stage breast cancer cases. As an example, OHSU only uses INTRABEAM™ for early stage breast cancers for patients within the criteria listed above, which amounts to 15 to 25 patients a year. We feel by researching the performance and side effects associated with dose from this device, we can provide evidence based research that ensures patient safety while expanding the use of IORT.

The low energy x-rays that INTRABEAM™ uses to deliver radiation is known to have a sharp drop off of dose in tissue with distance from the INTRABEAM™ applicator, shown in Fig. 2.2. This sharp drop off is an advantage over EBRT because it reduces side effects primarily to effects from skin radiation exposure. Thus, measuring the skin toxicity with IORT is a high priority in order to anticipate, manage, and reduce dose effects that can range from skin irritation to dry or moist desquamation as well as subcutaneous fibrosis also seen from EBRT.

2.5.6 X-Ray Source Probe

The x-ray source(XRS) probe for the INTRABEAM™ device produces 50 kV x-rays (50kVp/40μA) or 40 kV x-rays (40kVp/40μA) at the end of 10 cm long tube that electrons travel down and strike a gold target. The tip of the unit is surrounded by a beryllium window allowing x-rays to pass and is covered with a thin film of nickel.

The isodose lines for the XRS probe are concentric spheres centered at the tip of the x-ray source (Biggs, 2006). The spherical isodose lines are achieved with a dithered beam allowing electrons to scatter uniformly around the tip.

The spectrum of x-rays from the 50 kVp output of the INTRABEAM™ is a typical

Figure 2.2: The spherical applicator attached to the INTRABEAM™ XRS probe which is attached to the base unit. The applicators come in a range of sized based on the tumor size and oncologist discretion. *www.meditec.zeiss.com/intrabeam.*

x-ray distribution with a maximum value of 50 keV and four overlying peaks (Biggs, 2006). The peaks at the low end of the spectrum are characteristic L lines from gold at 14.353 keV, 13.739 keV, and 11.925 keV, and the K line from the nickel coating at 8.339 keV (Kaye & Laby Table of Physical & Chemical Constants, 2012). The overall broad spectrum is due to bremsstrahlung radiation from the target. The 40 kVp output distribution also has the four characteristic peaks from Gold and Nickel but with a maximum value at 40 keV.

Published results on the constancy of the output from the XRS probe show a decreases in output by 10% in a five year study where 9% of the output drop occurs in the first 200 days (Biggs, 2006). Even though the XRS unit is serviced every year, a large

portion of the decline in output occurs within the time frame of a service year. Even though the decrease in output is large during the first 200 days, the change in output is accounted for during treatment by adjusting the time the device delivers x-rays.

2.5.7 Preparing for INTRABEAM™ Treatment

If a patient falls within the patient criteria and their oncologist feels they will benefit from an INTRABEAM™ treatment, a medical physicist must perform pre-treatment quality assurance and output measurements to ensure the correct dose is delivered to the patient.

The INTRABEAM™ comes with a host of specific tools to aid the medical physicist. Four tools are available from the vendor to ensure the quality of the x-ray beam, namely a water phantom, a probe ionization/adjuster chamber holder (PAICH) system, a photodiode array(PDA) unit, and an ion chamber. All the tools are included with the INTRABEAM™ system except for the water phantom.

Water Phantom

The water phantom allows the determination of the depth dose curve for an XRS. The water phantom is made specifically for the XRS unit and allows tip of the unit to move in three directions and can be turned 360° along the Z axis. Most clinics do not have the water phantom and rely on the depth dose curve produced by the manufacturer.

The water phantom houses a solid water construction that holds an ion chamber. During measurements for the depth dose curve, the manufacturer collects current read-

ings from the ion chamber as the XRS unit is moved from 3 mm to a depth of 45 mm along the Z axis. Equation(2.29) corrects the raw ion chamber measurements in amps for changes in temperature and pressure from the conditions it was calibrated. The manufacturer than uses equation(2.30) to determine the dose rate in Gy/min at the specific depth of the ion chamber. The constants $N_s[R/C]$, k_Q, and $f[R/Gy]$ are the exposure calibration factor, the quality conversion factor, and the roentgen to gray conversion factor.

$$I_{T,p}(z) = I(z)\frac{T}{295.2K}\frac{760torr}{p} \tag{2.29}$$

$$\dot{D}_W(z) = I_{T,p}(z)[A]N_s[R/C]k_Q f[Gy/R]60[s/min] \tag{2.30}$$

Probe Ionization/Adjuster Chamber Holder

The probe ionization/adjuster chamber holder(PAICH) measures and adjusts the probe manually. This apparatus also contains an internal thermometer for temperature correction. The PAICH system also allows the mount of an included PTW soft x-ray ionization chamber(model 23342) within a manufacturer fabricated stage.

Photodiode Array

The photodiode array that comes with the system contains five photodiodes which measures the isotropy of the beam from the tip. When the XRS is emitting radiation,

the photodiodes collect current readings at different locations within the cylinder to determine the dose at the diode positions. The isotropy of the dose distribution is then determined from the diode readings.

Ion Chamber

The PTW soft x-ray ion chamber is a parallel plate ion chamber design and has a collection volume of 0.02 cm^3. The calibration for the device is performed at energies of 15 kV to 70 kV. It has been noted that this model of ion chamber has a flat dose response between 10 kV and 100 kV.

The ion chamber does not provide the absolute dose rate in water or tissue at any depth. The ion chamber collects charge in air measurements from the XRS while held in place with the PAICH system. These measurements are then compared to the readings from an identical measurement done with the XRS unit at the manufacturer's site, thus determining a correction factor.

2.5.8 Ion Chamber Quality Assurance

The heavy reliance on the functionality of the dedicated soft x-ray ion chamber leaves the INTRABEAM™ susceptible to errors in treatment if the performance of the ion chamber diminishes. If the ion chamber were to malfunction and report a current read too low, then the time of treatment would increase causing an over dose to the patient.

As an application for the nanoDot™ dosimeter, we examine a method that can used to verify the correct operation of the low energy x-ray ion chamber. A cross calibration

between a nanoDot™ dosimeter and the x-ray ion chamber based on the output of the XRS probe could easily provide a constancy check for the ion chamber that could be performed at the time the rest of the system is tested adding only a minimal amount of time.

The output check during the quality assurance tests uses the XRS probe for a specified duration of the time, approximately 2 minutes. Although the exact time is not known, the test is software controlled and is constant every time this procedure is performed. During this test, the soft x-ray ion chamber is collecting current information to determine the dose rate for the XRS probe. Replacing the ion chamber with a nanoDot™ dosimeter and performing the test again, the dose will be collected and can be read out from the dosimeter. Even though the exact time the XRS probe is in use during this test is not known, one could divide the dose rate obtained from the ion chamber measurement by the counts from the dosimeter measurement that would give a constant number over the course of multiple tests and be independent of the output changes of the XRS probe.

2.5.9 Distance Measurements

The INTRABEAM™ applicator is placed within the patient during treatment instead of going through the skin with conventional external radiation treatments. The surface skin dose may be lower for INTRABEAM™ treatments compared to external beam treatments because radiation from INTRABEAM™ may not even reach the surface skin. Of course, the potential hazards of exposure to vital organs exist for both treat-

ments. And, the high prescribed dose and long beam on time during treatments for the INTRABEAM™ could be considered a greater possibility of serious repercussions in the event of miscalculation or alignment compared to a single fraction mishap for external beam irradiation.

Measurements of the amount of dose is administered at different distances from the applicator of the INTRABEAM™ system leads to a better understanding of the dose distribution during treatment in particular the dose fall off gradient. With a better understanding of the dose gradient, the ability to predict the surface dose given the depth of a tumor bed will lead to a better prediction of the skin toxicity. The criteria for suitable patients based on tumor placement may be extended when the surface dose is correctly determined. At the very least, nanoDot™ dosimeters that measure the skin dose during treatment can help determine patient follow up care based on side effects predicted by the surface dose.

Table 2.1: ASTRO Criteria for INTRABEAM™ Patient Eligibility

Factors	Criterion
Patient Factors	
Age	$\geq$ 60y
BRCA1/2 Mutation	Not Present
Pathologic Factors	
Tumor Size	$\leq$ 2 cm
T Stage	T1
Margins	Negative by at least 2 mm
Grade	Any
LVSI	No
ER Status	Positive
Multicentricity	Unicentric Only
Multifocality	Clinically Unifocal with Total Size $\leq$ 2 cm
Histology	Invasive ductal or other favorable subtypes
Pure DCIS	Not Allowed
EIC	Not Allowed
Associated LCIS	Allowed
Nodal Factors	
N Stage	pN0(i-,i+)
Nodal Surgery	SN Bx or ALND
Treatment Factors	
Neoadjuvant Therapy	Not Allowed

3 Methods

3.1 Angular Dependence

A major concern throughout all of the experiments is the angular dependence for dose measurements the commercial OSL dosimeters display. Although our experiments are not designed to determine the dose response angular dependence, it is taken into account when we designed our experiments. As the face of the dosimeter is through 360° rotated relative to the central irradiation beam axis, the dose response will at most be lessened by 4% with 6 MV and 18 MV photons.[Kerns *et al.*, 2011] The maximum decrease in signal is found at angles 90° and 270°.However, it must be stated that earlier work has shown that for 6 MV angular dependence does not exist.[Jursinic, 2007] At 80 kVp and 120 kVp energy irradiations, the decrease in dose response at 90° is 40% and 20% respectively. Needless to say, there is a higher angular dependence on dose measurements as irradiation energies decrease.

In our experiments, we carefully and consistently make sure the normal to the face of the dosimeter is parallel to the central irradiation beam access. Our experimental design is developed with the easiest way to ensure repeatability in setup. In cases the case where dosimeters are placed with an offset, but the normal of the dosimeter is still parallel to the central axis, the offset is at most 5cm. Considering the 5 cm offset and the greatest source to dosimeter distance being 103.5 cm, the angle of irradiation is at

most is 2.77°. Since the offset is only used for 6 MV, 10 MV, and 18 MV photon beams, the decrease would be less than a half a percent considering at 45° for these energies the decrease is less than a percent.

3.2 Common Experimental Equipment

3.2.1 Commercial OSL Dosimeters

Throughout these experiments, we use the nanoDot™ OSL dosimeters (Ladauer, Inc., Glenwood, IL). The OSLDs have an active crystal region of aluminum oxide doped with carbon (Al_2O_3:C) that measures 5 mm in diameter and < 1 mm thick. The encapsulation of the active region is a durable light tight casing adding dimension to the OSL dosimeters for an overall size of 1 cm $\times$ 1 cm $\times$ 0.2 cm.

The manufacturer provides nanoDot™ OSL dosimeters with two types of accuracy of 5% and 2% as determined through irradiation experiments. The OSL dosimeters in these experiments are pre-screened by the manufacturer and purchased as devices with accuracy of 2%. The manufacturer also claims their devices are applicable for energy ranges of 5 keV to greater than 20 MeV.

These OSL dosimeters have experimentally shown to have a dose response which is linear below 200 cGy and then the response becomes supra-linear (Jursinic, 2007). The nanoDot™ OSL dosimeters have also been shown to have neither an angular dependence nor temperature dependence for MeV photons(Jursinic, 2007).

3.2.2 microStar® InLight® Reader

The microStar® InLight® Reader manufactured by Landauer, Inc. (Glenwood, IL). The reader is approximately 30 $\times$ 20 $\times$ 10 cm^3 and houses 36 LEDs that emit 532 nm as the stimulating source. The dosimetry reader can use two different intensities of light to stimulate the OSL dosimeters. The necessity for two intensities of light is a direct result of saturation of the photomultiplier tube (PMT) at high counts and the desire to increase the signal to noise for low counts. The strong signal provides stimulation for lower doses (< 10 cGy) while the weak signal stimulates the OSL dosimeters for higher doses (> 10 cGy) according to the manufacturer.

The microStar® InLight® Reader relies on two calibration curves to convert counts to dose. For counts that result in doses below 200 cGy, a linear calibration curve best models the dose response shown in EQ.(3.1), which shows that dividing the counts by the calibration factor (C.F.) and sensitivity(S) gives the dose.

$$Dose = \frac{Counts}{C.F. \times S} \tag{3.1}$$

For counts that result in a dose higher than 200 cGy, the reader software uses a non-linear calibration curve to convert the counts to dose that has the functional form shown in EQ(3.2). The calibration factors and calibration coefficients used in the experiments are shown in Table(4.1). The calibration factors and coefficients derived from the single use dosimeter calibration method and the non-linear calibration curve has a range of 0 cGy to 1300 cGy.

$$Dose = a \left(\frac{Counts}{S}\right)^2 + b \left(\frac{Counts}{S}\right) + c \tag{3.2}$$

Table 3.1: Parameters for Calibration Curves

Experiment	Constant
Linear	
Strong Intensity	7547.437
Weak Intensity	644.832
Non-Linear	
a	-1.59 $\times 10^{-10}$
b	1.47 $\times 10^{-3}$
c	2.926

3.2.3 IBA Farmer Ion Chamber

An IBA Farmer Ion Chamber, model FC65-G, measures the absolute dose for experiments requiring an ion chamber. The chamber is calibrated by K & S Associates, Inc. (Nashville, TN) and has a calibration factor of 4.895×10^7Gy/C. The ion chamber has a sensitivity of 21×10^{-9} C/Gy.

The absolute dosimetry allows a comparison of irradiations to the OSL dosimeters in the advent of changes to conditions or set up that may change the delivered dose. The presence of the ion chamber is considered with the design and setup of the phantom. The ion chamber is placed after the dosimeters and far enough away so it does not affect the irradiation of the dosimeters.

3.2.4 Soft X-Ray Ionization Chamber

For experiments where the energy ranges are between 10 kV and 100 kV, the PTW soft x-ray ionization chamber, model number 23342, is used for charge collection. The chamber has a charge collection volume of 0.02 cm^3 and is considered to have a flat response in the energy range of 10 to 100 kV. The chamber is vented making it necessary to make air density corrections to the raw measurements. The ionization chamber has a calibration constant of 1.178×10^9 Gy/C.

3.3 Experiments

3.3.1 Initial Experiments

Read Out Signal Depletion

This experiment uses dosimeters pre-irradiated to a known dose and then the dosimeters are read out a total of 25 times using the InLight® microStar® InLight® Reader. After irradiation, the dosimeters sit in a cardboard box in a dark room for 10 minutes to allow the shallow traps to clear themselves if necessary.

After reading the dosimeters 25 times, the dose readings are normalized to the first reading and plotted as a scatter plot of dose verses read out iteration. The linear trend is modeled using a linear regression fitting in Microsoft Excel (2010) and confirmed with the statistical software R© (The R Foundation for Statistical Computation, Version 2.15.2, 2012).

Dose Response

This experimental set up is also used in other experiments which will be outline in their respective sections. A Trilogy linear accelerator (Varian Medical Systems, Palo Alto, CA) is the 6 MV photon source for all irradiations. The linear accelerator is calibrated at 6 MV to have d_{max} of 1.5 cm where 1 MU is equivalent to 1 cGy by guidelines outlined in TG-51.[Almond *et al.*, 1999]

This experiment requires a phantom that uses a combination of solid water and tissue equivalent bolus slabs manufactured by Civco Medical Solutions (Kalona, IA) as buildup and backscatter materials, shown in Fig.(3.1).

Figure 3.1: Three nanoDot™ dosimeters are placed in between two bolus slabs at the 8 cm mark and at the 17.5 cm mark is a hole for the 0.65 Farmer ion chamber. The phantom is irradiated with a 6 MV photon beam at an SSD of 100 cm and 10×10 cm^2 field size.

The orientation of the OSLDs during irradiation places the normal of its flat face parallel to the central axis of the x-ray beam. The depth of the OSL dosimeters is at 1.5 cm, d_{max}. Due to the profile of the beam at d_{max}, the measurements are 2.5 cm from

the central axis of a 10×10 cm^2 field, which is shown in Fig.(3.2). With a farmer ion chamber at 10 cm depth, a minimum of 6.5 cm of backscatter material exists after the OSL dosimeters. An additional 5 cm of backscatter material exists after the ion chamber for accurate readings.

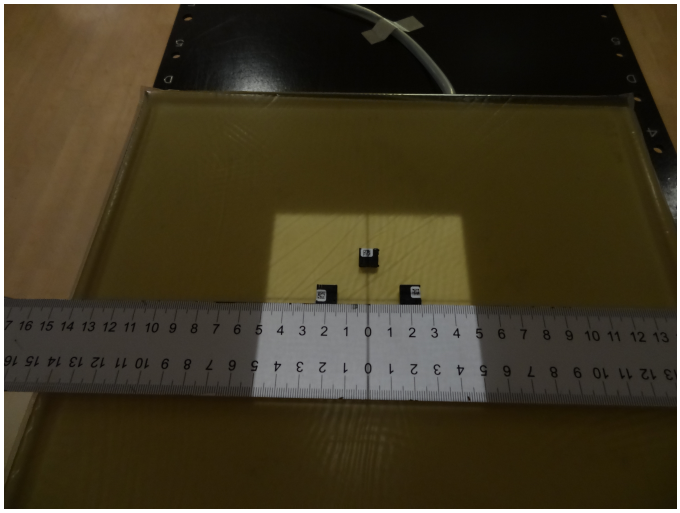

Figure 3.2: The off central axis placement of the nanoDot™ dosimeters is due to a slight dip in the beam profile at 1.5 cm. The nanoDot™ dosimeters are placed at 2.5 cm from the central axis on a bolus slab in a 10×10 cm^2 field.

This experiment uses three nanoDot™ dosimeters during the irradiation process and reports the results of all three nanoDot™ dosimeters. Once placed between the two bolus slab at 1.5 cm depth, the dosimeters undergo a series of irradiations and readouts. The dose increments are 0, 10, 30, 50, 80, 100, 150, 200, 300, and 400 cGy and after 400 cGy they increment by 200 cGy until 3800 cGy. Once the nanoDot™ dosimeter has been irradiated, it sits in a dark room for 10 minutes before being readout.

A linear curve is generated from the measured points below 200 cGyusing a linear regression algorithm found in Microsoft Excel (2010). The linear curve is used as a

reference curve to see the changes in linearity in the dose response

Calibration Curve

Two methods exist for generating a calibration curve for OSL dosimeters. Both consist of irradiating the dosimeters to known doses and then reading out their counts. However, one method uses new dosimeters for each irradiation point while the other uses the same dosimeters for all dose points allowing the dose to accumulate on the device.

Our experiment irradiates groups of commercial OSLDs to different dose amounts with 6 MV photons from a Novalis TX linear accelerator (Varian Medical System, Inc., Palo Alto, CA) at an SSD of 100 cm and the field size to 10 x 10 cm^2. The phantom setup consists of the nanoDot™ dosimeters sitting between two 1 cm thick water equivalent bolus material slabs with 5 cm of solid water (Civco Medical Solutions, Kalona, IA) used as back scattering material. On top of the bolus lies an additional 0.5 cm solid water slab placing the dosimeters at a total depth of 1.5 cm from the surface.

For the single use nanoDot™ dosimeter calibration curve, one of eleven groups of three new OSL dosimeters are irradiated to the dose points of 0, 10, 100, 300, 500, 800, 1000, 1300, 1500, 1700, and 2000 cGy. After irradiation and a 10 minute waiting period, each of the OSL dosimeters in a group is read out three times. The counts for each reading are divided by the sensitivity for each individual dosimeter and the mean number of counts for the group is determined for a specific dose point.

The accumulative dose calibration curve irradiates three new nanoDot™ dosimeters to dose points of 0, 10, 100, 300, 500, 800, 1000, 1300, 1500, 1700, and 2000 cGy by supplying them with 10, 90, 200, 200, 300, 200, 300, 200, 200, and 300 cGy. After

each irradiation, each dosimeter is read out three times after a 10 minute waiting period. The average counts for all dosimeters is determined once the average for each individual dosimeter is divided by its sensitivity and reported as the counts for the specific dose.

Each data set is fit to a second ordered polynomial curve using a non-linear polynomial regression algorithm provided by Microsoft Excel (2010), which has been shown to produce the same results as the microStar® InLight® Reader Software (Landauer, Inc., Version 4.3). The algorithm gives the fit constants labeled a, b, and c for the second order polynomial equation, $y = ax^2 + bx + c$, along with an R^2 value rating the fit.

3.3.2 Optical Bleaching

The optical bleaching experiment uses eight groups of pre-irradiated commercial OSL dosimeters. Although the individual accumulative dose amount is known for each dosimeter, the doses are not the same for the three dosimeters in each group. Therefore, the percentage of the original dose remaining on a dosimeter is reported.

Each measurement of dose on a dosimeter is performed three times for each dosimeter and an average for that dosimeter reading is determined. In this manor, an initial dose is determined for all dosimeters used in the experiment. Then, three random dosimeters are assigned to a group destined to receive different amounts of bleaching time. The dosimeters are opened to expose their active crystal region and placed on a light box which exposes them to light from a 15 W fluorescent lamp, shown in Fig.(3.3)

Each group has a different bleaching time, which are incremented by ten minutes producing bleaching times of 10, 20, 30, 40 , 50, 60, 70, 80 minutes. After the bleaching

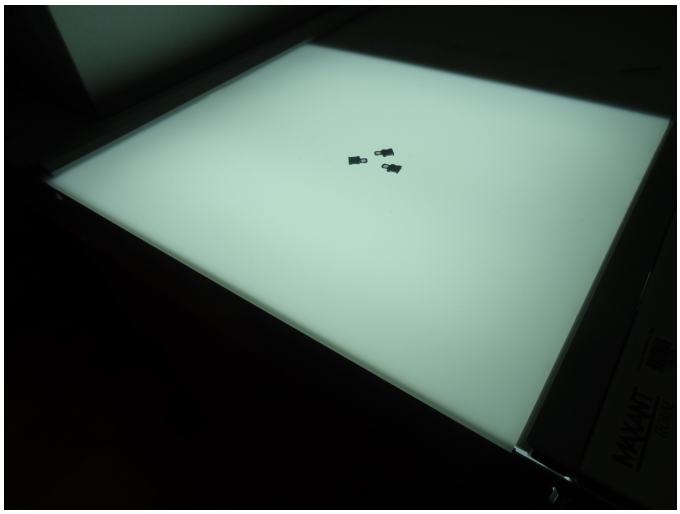

Figure 3.3: Three opened dosimeters placed on a light box which exposes them to light from a four 15 W compact fluorescent lamps.

time, each group is removed from the light box and placed in dark box for ten minutes before read out. Each OSL dosimeter is read out three times to obtain a final dose.

Given the average initial dose and average final dose for each individual dosimeter, the percentage of original remaining dose can be determined. Once the percentage of original remaining dose is determined for all dosimeters in a group, the average for the group is calculated.

The analysis of the data determined its linearity after a log-log transformation using a Q-Q Plot. The linear regression of the log-log transformed data is then back transformed to determine a power fit with the variables of interest, namely time and percent of original remaining dose. The statistical analysis is performed with the statistical software R© (The R Foundation for Statistical Computation, Version 2.15.2, 2012).

3.3.3 Repeatability

For this experiment, a Trilogy linear accelerator (Varian Medical Systems, Palo Alto, CA) is the 6 MV photon source for all irradiations. The linear accelerator is calibrated at 6 MV to have d_{max} of 1.5 cm where 1 MU is equivalent to 1 cGy by guidelines outlined in TG-51(Almond *et al.*, 1999).

This experiment requires a phantom that uses a combination of solid water and tissue equivalent bolus slabs manufactured by Civco Medical Solutions (Kalona, IA) as buildup and backscatter materials, shown in Fig.(3.1).

The orientation of the OSLDs during irradiation places the normal of its flat face parallel to the central axis of the x-ray beam. The depth of the OSL dosimeters is at 1.5 cm, d_{max}. Due to the profile of the beam at d_{max}, the measurements are 2.5 cm from the central axis of a 10×10 cm^2 field, which is shown in Fig.(3.2). With a framer ion chamber at 10 cm depth, a minimum of 6.5 cm of backscatter material exists after the OSL dosimeters. An additional 5 cm of backscatter material exists after the ion chamber for accurate readings.

In these experiments, we use our method for optically bleaching nanoDot™ dosimeters with a light box to remove dose in conjunction with 100 cGy irradiation to observe their dose response after bleaching. This experiment is designed to compare the 100 cGy dose response between nanoDot™ dosimeters that have been optically bleached after irradiation and ones that have not been bleached.

Six new nanoDot™ dosimeters are irradiated with 100 cGy with 6 MV photons from the linear accelerator described above. After the first irradiation of 100 cGy, the

nanoDot™ dosimeters are read out three times using the microStar® InLight® Reader and an average is determined for each dosimeter. Once read out, three dosimeters are optical bleached for 2 hours. These dosimeters are then read out a second time to obtain their current dose level. All six dosimeters are then irradiated with another 100 cGy and read out. This process is repeated 20 times and the dose is determined by subtracting the average initial dose from the average final dose for each individual dosimeter.

The uncertainty in the dose measurements is determined by calculating the 1-sigma standard deviation for each dosimeter based on the three reading of each irradiation. For the non-optically bleached dosimeters, the error of the initial and final dose reading is propagated to the dose difference. The the dose, $u(m_1, m_2)$, which is a subtraction of two values, m_1 and m_2 is dependent on the numerical reading of each value and its uncertainty. The uncertainty in the dose can be calculated using EQ.(3.3) and for the simple case of a calculating a difference, the uncertainty is given by EQ.(3.4).

$$\sigma_u^2 = \left(\frac{\partial u}{\partial m_1}\right)^2 \sigma_{m_1}^2 + \left(\frac{\partial u}{\partial m_2}\right)^2 \sigma_{m_2}^2 \tag{3.3}$$

$$\sigma_u = \sqrt{\sigma_{m_1}^2 + \sigma_{m_2}^2} \tag{3.4}$$

The same procedure is repeated using six new nanoDot™ dosimeter for both 10 MV and 18 MV energies. The phantom set up changes for each of the energies because the depth of maximum dose is deeper for higher energies. The dosimeters are therefore placed at 2.5 cm for the 10 MV photon beam and 3.5 cm for the 18 MV photon beam. In each case, the ion chamber remains at 10 cm depth and the dosimeters are placed

between two 1 cm thick bolus slabs.

3.3.4 Low Dose Sensitivity Changes

This section explains our experiment designed to explore the sensitivity changes in commercial OSL dosimeters based low accumulative dose. In this experiment four new dosimeters are used. Each of the four dosimeters have a different accumulative dose, namely 0, 10, 20, and 30 Gy.

The doses are delivered to the dosimeters with 6 MV photons from a Trilogy linear accelerator (Varian Medical Systems, Palo Alto, CA) with an SSD of 100 cm and a 10×10 cm^2 field. The linear accelerator is calibrated at 6 MV to have d_{max} of 1.5 cm where 1 MU is equivalent to 1 cGy by guidelines outlined in TG-51(Almond *et al.*, 1999).

The nanoDot™ dosimeters are placed at a depth of 1.5 cm. The dosimeters are in between to tissue equivalent 1 cm bolus slabs with an additional 0.5 cm solid water sheet on top to create the correct depth. Solid water slabs are then places below the bolus to create 5 cm of backscatter material. At 10 cm depth, an farmer ion chamber is placed and then an additional 5 cm of backscatter material is added to complete the phantom set up.

For all irradiations, ion chamber measurements are taken to ensure the correct dose is delivered to the dosimeter. The farmer chamber has a volume of 0.65 cm^3 and reports the amount of charge collected during the irradiation in nC. Before dosimeter irradiation, the chamber is irradiated multiple times with 100 monitoring units to allow the chamber

to equilibrate. In this manor, a conversion factor relating ion chamber readings to dose at 1.5 cm depth and is 7.18 cGy per nC. It has been determined based on ion chamber readings all irradiations vary with an average of 0.5% of the intended dose.

After the experimental set up is complete and the ion chamber is equilibrated, three of the four dosimeters are dosed to their prescribed amount. Each dosimeter is placed at 1.5 cm depth and irradiated to 10, 20, and 30 Gy as confirmed with the ion chamber reading. The three dosimeters are then placed in a light box housing four 15 W CFLs for optical bleaching. The dosimeters optically bleached for 72 hours reducing their dose to less than 0.02 cGy, which is comparable to the dose of new nanoDot™ dosimeters from the manufacturer.

The four nanoDot™ dosimeters are then placed at 1.5 cm within the experimental phantom. The dosimeters are undergo a series of irradiations and read outs to establish the dose response at low doses. The dosimeters are irradiated with 10, 20, 20, 30, 20, 50, 50, 50, 50 cGy producing total doses of 10, 30, 50, 80, 100, 150, 200, 250, and 300 cGy.

Comparing Linear Calibration Curves

The linear calibration curves can be compared by combining the individual data sets and introducing a new variable. As one combined data set, the points are distinguished by the new dummy variable which signifies whether the data point is from data set 1 or data set 2. For ease of use, the variable takes on the values of 0 or 1 to identify which data set the point is from.

With the introduction of the new dummy variable, a single linear model can be used

for the entire data set that has a cross term as shown in EQ.(3.5). In this case, the independent variable is x and the dummy variable is z.

$$y = \beta_0 + \beta_1 x + \beta_2 z + \beta_3 (x \times z) \tag{3.5}$$

An analysis of variance (ANOVA) can now be performed on the combined data set. The ANOVA test will reveal the strength of the null hypothesis or the alternative hypothesis testing whether the data sets are different enough for two curves or similar enough for a single curve. The ANOVA generates an $F - stat$ which is used in conjunction with the degrees of freedom for each data set and an F distribution to determine the p-value for our hypothesis. The null hypothesis stating the two are similar and only a single linear relationship is supported when the correlation term, $\beta_3(x \times z)$ in EQ.(3.5), is statistically unnecessary. In this case, z takes on the value of zero and the associated equation is $y = \beta_0 + \beta_1 x$ for the entire combined data set. If the null hypothesis is not supported, two linear curves are generated which model each data set separately. One data set is modeled when z is 0 and the other when z is 1.

All data sets could be combined allowing the z to uniquely specify data from each set of points. In the pursuit of simplicity, only two linear curve data sets were compared at a time and reduced the likelihood of errors.

Sensitivity Changes for Large Accumulative Dose

To understand how the sensitivity changes with accumulative dose, the sensitivity experiment is continued past 20 Gy to 160 Gy. The irradiation dose is also extended to 10

Gy per iteration instead of 100 cGy.

Three nanoDot™ dosimeters are irradiated with each iteration of 10 Gy for this experiment. Again, the doses are delivered to the dosimeters with 6 MV photons from a Trilogy linear accelerator (Varian Medical Systems, Palo Alto, CA) with an SSD of 100 cm and a 10×10 cm^2 field. The linear accelerator is calibrated at 6 MV to have d_{max} of 1.5 cm where 1 MU is equivalent to 1 cGy by guidelines outlined in TG-51(Almond *et al.*, 1999).

After irradiation, the dosimeters are placed in a dark room for 10 minutes and then read out three times. Once the read out with complete, the nanoDot™ are opened and placed in a light box with four 15 W CFL for two hours for optical bleaching. After the bleaching time, the dosimeters are read out three times to obtain the remaining dose. The cycle then repeats with an irradiation of 10 Gy. For each iteration, an average of the initial dose and final dose is determined from the three readings. The difference between the average initial and final dose is determined. The reported dose measurement is the differences in the averages and the 1σ standard deviation as the uncertainty.

3.4 INTRABEAM™ Applications

3.4.1 Ion Chamber Quality Assurance

Our method for performing a constancy check on the soft x-ray ionization chamber uses the quality assurance systems already in place for the INTRABEAM™ system. The system requires an output check before treatment using their dedicated probe ion-

ization/adjuster chamber holder (PIACH), software, and a dedicated electrometer. Our method uses the same setup and software to run the same test but with a nanoDot™ dosimeter in place of the ion chamber. The entire system setup with the ionization chamber in place is shown in Fig.(3.4).

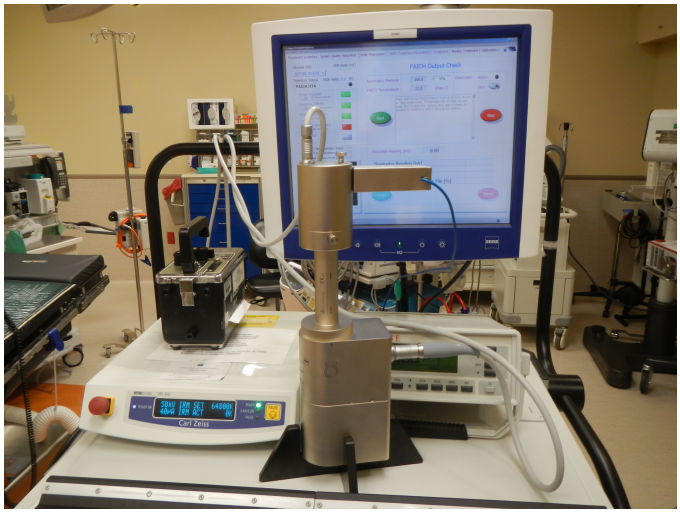

Figure 3.4: The INTRABEAM™ system set up for output quality assurance tests with the ionization chamber in the PIACH system.

The nanoDot™ dosimeter stage is constructed out of acrylonitrile butadiene styrene (ABS) plastic with a 25% fill using a 3-D printer in the Oregon State University Physics Department. The design of the stage is based on measurements of the ion chamber. The dosimeter stage is designed using AutoDesk® Inventor® Professional (2013). The final design places the center of the crystal region of the dosimeter at the center ion chamber collection plate. The dosimeter stage and the ion chamber are shown next to each other in Fig.(3.5).

The stage for the nanoDot™ dosimeter needs to match the dimension of the ionization chamber to ensure the correct placement of the dosimeter. Another reason for

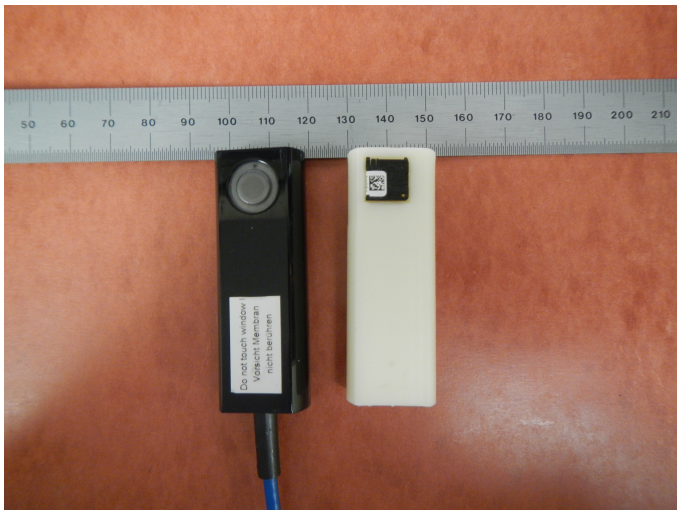

Figure 3.5: The nanoDot™ dosimeter stage and soft x-ray ion chambers used during the cross calibration experiment have the same dimensions.

the careful construction allows the use of the ion chamber holder with fits within the PIACH system. The holder and PIACH system provide shielding during the test. The nanoDot™ dosimeter stage within the ion chamber stage is shown in Fig.(3.6).

When the output test is run, the software has an interlock that uses feedback from the electrometer to ensure the system is running correctly. If a minimum current is not detected, the test stops assuming something is incorrectly setup. Since our set up does not use the electrometer, an external source is necessary to provide an amount of current for the electrometer. To overcome the minimum current interlock, we used an HDR 1000 Plus Well Chamber with three seeds of ^{125}I to produce a current of approximately 25 pA. Connecting the output of the well chamber to the electrometer provided enough current to override the interlock.

The data collection starts with using the ion chamber to determine the dose rate of the XRS probe. This portion of the experiment follows the quality assurance procedure,

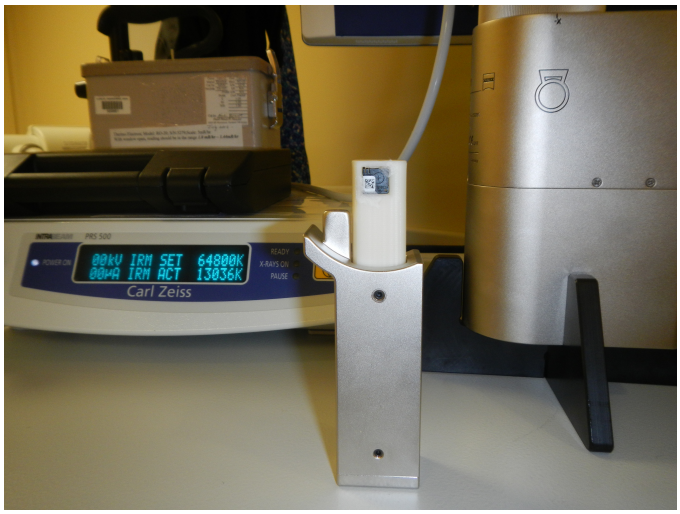

Figure 3.6: The nanoDot™ dosimeter stage fits within the ion chamber holder. The holder allows the use of the INTRABEAM™ PIACH system, which provides shielding during the experiment.

where the ion chamber collects current information for a duration of time. This current is then converted to a dose rate.

The data collection with nanoDot™ dosimeters is performed with three different dosimeters and using a 25% fill dosimeter stage. The radiation leakage during the experiment is non-existent as confirmed with an independently calibrated Geiger counter. Each irradiation period lasts for approximately 2.133 minutes, which includes a warm up period for the XRS probe. All interlocks were successfully placated during the experiment.

After irradiation, the nanoDot™ dosimeters are placed in a light tight envelope for 30 minutes to allow for any phosphorescences to subside. Then, each dosimeter is read out three times using the microStar® InLight® Reader. The counts collected from the reader are corrected by dividing the counts by the inherent sensitivity of the dosimeter as determined by the manufacturer. The corrected counts are then divided by the dose rate

reported by the ion chamber procedure. The average counts per dose rate is determined using all nine readings and a 1σ uncertainty is calculated for the average based on the nine readings.

As a comparison, two nanoDot™ dosimeters were irradiated with the same procedure, but a 35% fill stage is used to hold the dosimeters in place. The stage is constructed with the same design files as the 25% file stage except with a higher fill amount. Again, the two dosimeters are allowed to rest after irradiation for 30 minutes and read out three times. The collected counts are corrected with the sensitivity of each of the dosimeters, then divided by the dose rate, and averaged. The 1σ uncertainty is all calculated based on the six readings.

The last of this set of experiments uses the 25% fill stage to hold the dosimeters but the XRS probe is set to 40 kVp with 40 μA. The procedure for this experiment follows the experiment preformed at 50 kVp.

3.4.2 Distance Measurements

The three distance measurements are performed for both the nanoDot™ dosimeters and the soft x-ray ion chamber. The measurements are collected at distances of 0.2 cm, 0.5 cm, and 0.7 cm from the applicator surface. For these measurements, three new nanoDot™ dosimeters are used while the ion chamber is set to collect charge for each irradiation. The prescribed dose has been set to 5 Gy at the surface, which is a 15 Gy decrease in dose than what is usually prescribed for a patient receiving treatment. The decrease in prescribed dose decreases the treatment time from approximately 20 minutes

to 5 minutes. The irradiation is performed with a setting of 50 kVp at 40 μA. At the time of irradiation, the temperature reading is 22.0 °C with a pressure reading of 102.1 kPa leading to a temperature and pressure correction factor of 0.992.

The set up consists of using solid water slabs of 0.2, 0.5, and 0.7 cm thickness. The nanoDot™ dosimeters are placed within a holding stage made of acrylonitrile butadiene styrene (ABS) plastic with a 25% fill using a 3-D printer in the Oregon State University Physics Department. The stage is designed to the specifications of the ion chamber. While in the stage, the stage is taped to the solid water so the dosimeter is placed at the center of the slab. The stage is then placed on top of 2 cm of tissue equivalent bolus slabs for backscatter. To further support the solid water slab, 2 cm thick styrofoam is placed next to the stage in between the solid water and bolus slabs. The set up is shown in Fig.(3.7) for the nanoDot™ dosimeter stage without the solid water slab on top. The design of the set up is such that the nanoDot™ dosimeter stage and the ion chamber can easily be interchanged.

Once the set up is complete for either the nanoDot™ dosimeter stage or the ion chamber and a measurement is ready to be taken, the INTRABEAM™ applicator is placed in position. For these experiments, a 2.5 cm applicator is used. The applicator is placed in contact with the solid water the center of the solid water. This aligns the applicator with either the nanoDot dosimeter or the ion chamber on other side of the solid water.

During a patient treatment, the applicator is placed inside the patient and minimal external shielding is necessary. With applicator exposed, heavy lead shielding is used to limit the amount of exposure to the surrounding area. After the applicator is in place

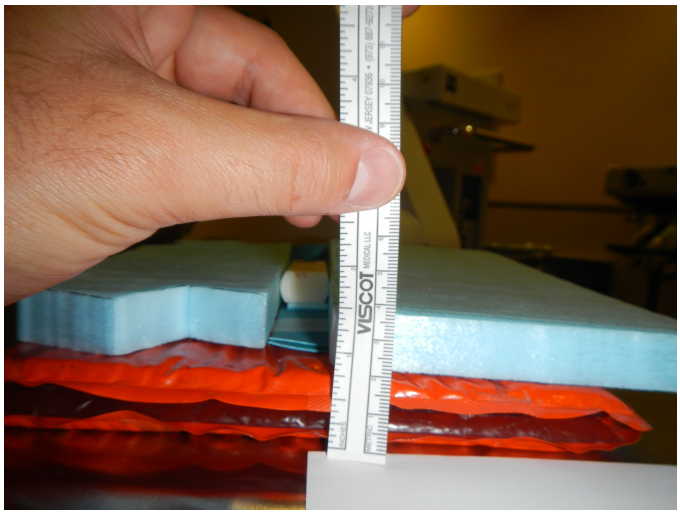

Figure 3.7: The nanoDot™ dosimeter is placed in an ABS plastic stage with 2 cm of bolus material behind it and 2 cm of styrofoam on either side.

lead is placed around the applicator as shown in Fig.(3.8).

The dose reading from the nanoDot dosimeters is determined the dose to counts conversion factor for 50 kVp energy determined during the ionization chamber quality assurance experiment, which is 284561 counts/Gy. After irradiation, each nanoDot™ dosimeter is placed in a dark box for at least 30 minutes. The dosimeters were then read out three times and an average of counts is determined for the dosimeter. Since only one dosimeter is used for each irradiation distance, the average becomes the reported dose at that distance. The dose from the ion chamber readings is determined by multiplying by the ion chamber calibration factor, then correcting with the temperature and pressure correction factor and the ratio of mass attenuation coefficients of water to air as shown in EQ.(3.6).

$$Dose[Gy] = MN_x P_{T,P} \left.\frac{\mu_{en}}{\rho}\right|_{air}^{water} \tag{3.6}$$

Figure 3.8: Lead shielding is used to limit the amount of exposure to the room. The lead is placed around the applicator.

The INTRABEAM™ x-ray probe produces an output of 18 keV at a depth of 5 mm of solid water (Armoogum *et al.*, 2007). The mass attenuation factors are listed in Kahn, 2007 for water and air for a 20 keV beam and the ratio is calculated to be 1.02. Even though the National Institute of Standards and Technology (NIST) gives values that are slightly different than those listed in Kahn, 2007, the ratio of NIST values is also 1.02.

3.4.3 Patient Data

The nanoDot™ dosimeters are placed on a patient when they receive intraoperative radiotherapy with the INTRABEAM™ system. Four nanoDot™ dosimeters are placed around the applicators insertion point. The set up is shown in Fig.(3.9) and the dosimeters are distinguished by color. This requires great deal of preparation because the whole procedure happens while the patient is still anesthetized.

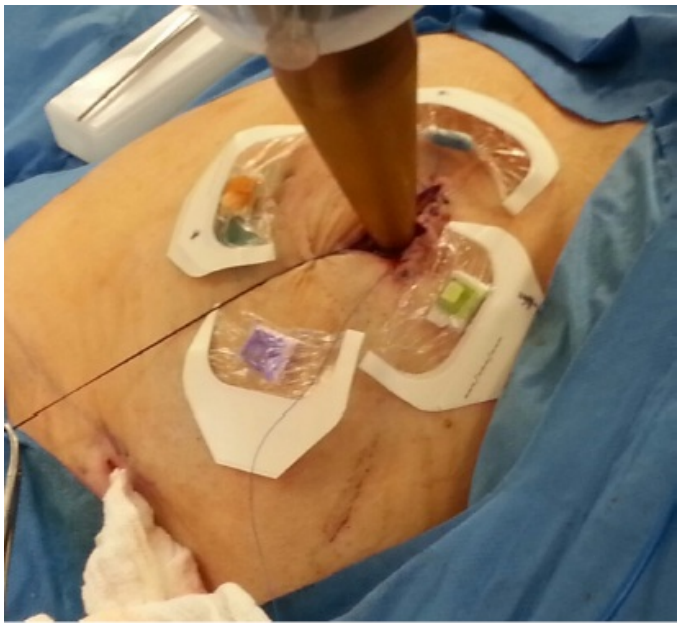

Figure 3.9: Four nanoDot™ dosimeters are placed on a surface of a patient around the INTRABEAM™ applicator. A picture is taken for each patient and the dosimeters are distinguished by color.

To determine the dose from the OSL dosimeter counts, we use the conversion factor of 284561 counts/Gy determined during the ionization chamber quality assurance experiment. The collection methods are not part of this thesis only the conversion of counts to dose. We did not perform the actual methods of collecting and placement of the dosimeters.

4 Results and Discussion

4.1 Initial Experiments

Read Out Signal Depletion

The results of our signal depletion experiment is summarized with Fig.(4.1), which shows the data for a single dosimeter with an initial average dose of 679 cGy and its 25 sequential readings. The linear fit to the data shows a slope of -0.0005 and an intercept of 0.997 after all the points have been normalized to the first reading. This data shows a reduction fraction after a single reading of 0.9995, which is equivalent to 0.05% reduction of signal per reading. Our reduction percent of 0.05% is in agreement with other authors who have looked at the depletion of signal on these OSL dosimeters and have reported reductions factors between 0.9993 and 0.9997 (Jursinic, 2007; Mrčela *et al.*, 2011).

The manufacturer reports a reduction percentage of 0.2%, which is much greater than the reported published data. However, it is concluded that the reported value from the manufacturer is from the use of the high intensity light, while our findings and other published data uses the low intensity light for stimulation.

Dose Response

The dose response for three nanoDot™ dosimeters is plotted for a dose range of 0 to

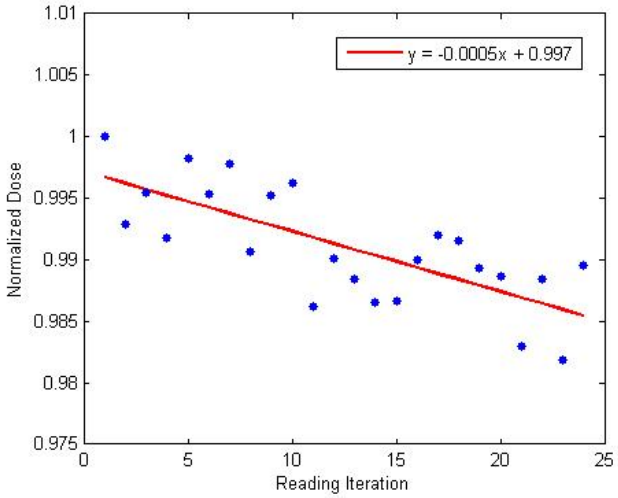

Figure 4.1: The degradation of signal on a commercial OSL dosimeter after sequential readouts is 0.05%.

38 Gy in FIG.(4.2). The curves are labeled based on the last four characters of each dosimeter serial number. The dose response is linear below 200 cGy and non-linear after 200 cGy which is noticeable when compared to the linear line also plotted on the figure. The linear line, $counts = 665.22 \times Dose - 778.79$, is a linear regression fit determined from all points below 200 cGy for nanoDot™ dosimeter 819A.

The initial linear response region followed by a non-linear region has been reported by other authors. Although our data shows the same general trend, the exact curves do not agree. This is expected because of variability seen between manufacturing batches and is usually explained as a result as changes in manufacturing condition between batches. However, our dosimeters show are more sensitive by two orders of magnitude from the published results of Jursinic in 2007.

The high variability raises questions of consistency in the manufacturing process of

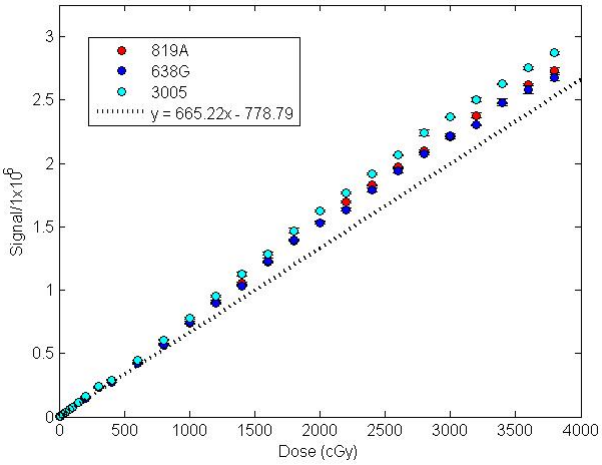

Figure 4.2: The dose response of the nanoDot™ dosimeters is linear below 200 cGy and then becomes non-linear after 200 cGy. The dosimeters are named based on the last four characters in their serial number.

these devices. And, if the variability is so high, do calibration curves translate well from one batch to another. One could argue that the amount of points in our fit is greater limiting the fit of the published data which only has a dose range of zero to 1000 cGy. However, the actual data points don't agree between our data set and theirs, which rules out the accuracy of the fit. For example, at 1000 cGy they report 1.4×10^6 counts and we report 0.65×10^6 counts.

Calibration Curve

Each one of the four calibration curves shown in Fig.(4.3) are produced from subsets of the single use data set that ranges from 0 to 2000 cGy. The 2000, 1700, 1300, and 1000 cGy curves are labeled for the highest dose point used to generate the curve. The subset of data points is fit to a second ordered polynomial curve using the non-linear

polynomial regression algorithm from Microsoft Excel (2010). The curve is then plotted for 0 to 2×10^6 counts in increments of 2.5×10^5. The greatest difference in reported dose for counts is 26.2% when comparing the 2000 cGy and the 1000 cGy curves at 2×10^6 counts. However, even comparing the 1300 cGy to the 2000 cGy curves has a difference of 4.74% in dose.

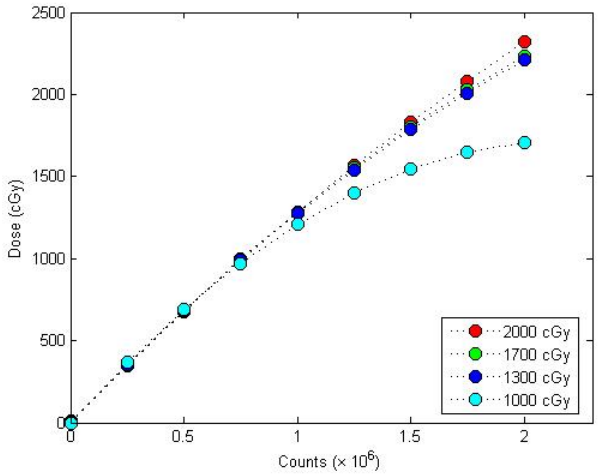

Figure 4.3: The single use dosimeter calibration curve changes depending on the dose range. Significant errors can occur if the calibration curve is extended past its dose range.

The same curves are generated for Fig.(4.4) using subsets of the data set generated with the accumulative dose method. The same non-linear polynomial regression algorithm from Microsoft Excel (2010) produces the calibration curves. The greatest difference in reported dose occurs at 2×10^6 counts between the 1000 cGy and the 2000 cGy curves where the difference is 13.1%.

In Fig.(4.5), we compare the entire data set for both the single use and the accumulative dose calibration curves and the fitting constants are given for both curves in Table (4.1). The two curves show some similarities for counts under 1×10^6 but at greater

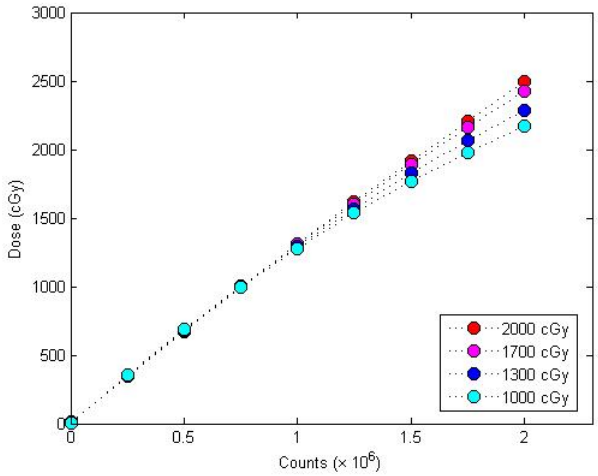

Figure 4.4: The accumulative dose calibration curve shows a decreasing sensitivity for doses outside the range of a calibration curve.

counts the two curves separate. At 2×10^6 counts, the dose reported from the two curves has a percent difference of 7.37%.

Table 4.1: Non-Linear Calibration Curve Parameters

Calibration Constants	Single Use Curve	Accumulative Dose Curve
a	-1.24×10^{-10}	-0.57×10^{-10}
b	0.001402	0.001356
c	7.82	9.77
R^2	0.9992	0.9998

Our analysis shows that extrapolating a calibration curve beyond the dose range from which it was generated will lead to erroneous dose readings. It is recommended that the manufacturer procedure be extended by multiple points beyond 1300 cGy to 2000 cGy when forming a non-linear calibration curve. This will ensure an accurate reading for the entire range for which the OSL dosimeters are reportedly useful.

It must be stated that a non-linear fit is only accurate for doses above 200 cGy. For

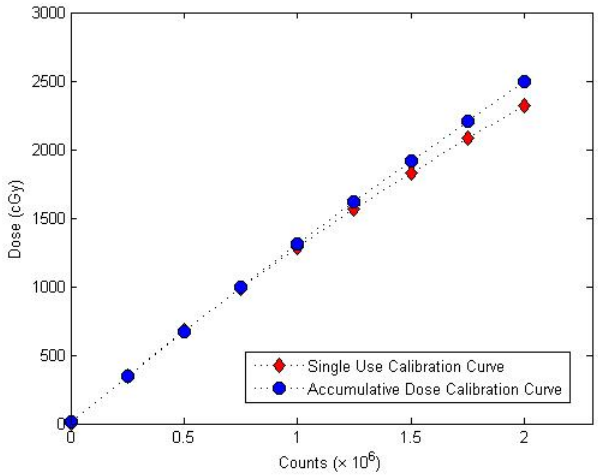

Figure 4.5: The accumulative calibration curve shows a higher dose corresponding to the count for a lower dose on the single use calibration curve.

example, the single use 2000 cGy calibration curve gives a dose reading of approximately 7.82 cGy for zero counts and the 1000 cGy calibration curve reports -1.65 cGy for zero counts. It is expected that the some background count are present, but if the OSL dosimeter is intended to be used for a dose below 200 cGy, a separate linear curve should be generated following manufacturer recommendations. Also, if the doses are subtracted in the case of repeated use of a dosimeter, the constant term has zero impact on determining the final dose.

Our calibration curves should not be taken as absolute calibrations, but as examples of a general trend when extrapolating calibrations curves beyond their dose range. Each institution should generate their own curves for the dose range they are interested in using the nanoDot™ dosimeters. It is important to also mention that we are only extending the manufacturer recommended dose points for the formulation of a non-linear calibration curve. One wonders why doses within the known linear dose response region would

be considered for fitting a non-linear curve. A piecewise function, linear below 200 cGy and non-linear above 200 cGy, may be the best for producing an accurate dose reading. Whether a piecewise function is used or not, a difference would be expected if one uses either the single use method or the accumulative dose method because of the sensitivity change of the nanoDot™ dosimeters associated with accumulating dose.

4.2 Optical Bleaching

The measurements of remaining dose on nanoDot™ Dosimeters for the eight groups are listed in Table(4.2). The data is plotted in Fig.(4.6) along with the curve fitting of the data. The data is fitted with a power curve of $y = 2.67.7t^{-1.39}$ and holds for optical bleaching times greater than 10 minutes. It is estimated that when the bleaching time is doubled, the median percentage of remaining dose of a commercially available OSL dosimeter changes by a factor of 38.15% (95% CI: 36.67% to 39.47%).

Table 4.2: Optical Bleaching Dose Reduction

Group	Bleaching Time (min)	% of Dose Remaining
A	10	10.75±0.28
B	20	4.08±0.27
C	30	2.38±0.35
D	40	1.70±0.34
E	50	1.21±0.22
F	60	1.02±0.03
G	70	0.66±0.07
H	80	0.58±0.02

The most efficient method of optically bleaching nanoDot™ dosimeters might be

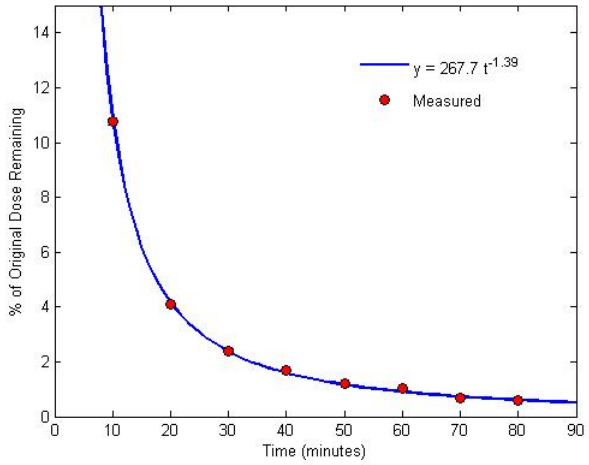

Figure 4.6: The reduction of original accumulated dose remaining on a commercial OSL dosimter after optical bleaching with light box that houses four 15 W CFLs can be fitted to $y = 2.67.7t^{-1.39}$ for t >10 minutes.

with a Tungsten-halogen lamp, which has been reported to remove 98% of dose in 45 s (Jursinic, 2007). Our method does not compare to the reported bleaching abilities of the Tungsten-halogen lamp, but efficiency is not our goal. However, our method reduces the dose on a dosimeter faster than bleaching with a bright room light. In one hour, our method can reduce the dose on a nanoDot™ dosimeter by 99% its original dose. Using just a room with a bright light,2 hours are needed to reduce the dose by 93% (Jursinic, 2007).

4.3 Repeatability

We present the absolute dose measurements for our repeated measurements using both the optical bleaching method and accumulative dose method for repeated use measurements from a 6 MV photon beam in Fig.(4.7). Each of the data points represents the

average reading of three nanoDot™ dosimeters read out three times. The data sets show readings of absolute dose can exceed the 5% as shown by the dashed lines which are at 100, 95, and 105 cGy.

The individual dosimeter readings for the repeated dose measurement experiment are shown in Fig.(4.8) with bin sizes of 2 cGy. Each data set consists of twenty points for each dosimeter for a total of sixty points. The optically bleached data set has a mean of 105.02 cGy with a standard deviation of 1.55 cGy. The accumulative dose data set has a mean of 103.97 cGy and a standard deviation of 5.13 cGy.

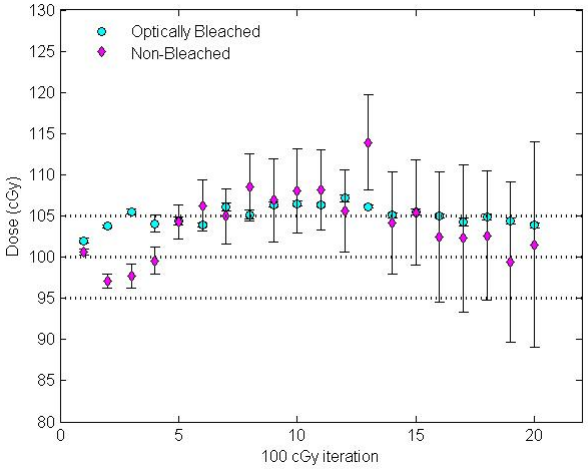

Figure 4.7: The absolute dose reading for optical bleached nanoDot™ dosimeters and non-optically bleached dosimeters for 20 iterations of 100 cGy for a 6 MV photon beam. Dashed lines represent 95, 100, and 105 cGy.

The data in Fig.(4.7) show a curved tendency of the repeated measurement that may suggest structure. In 2011, Mrčela *et al.* have performed this experiment for a dose range of 0 to 800 cGy and conclude that the data fit a second ordered polynomial after normalizing the data. Our data can be fitted to such a polynomial; however, the fit

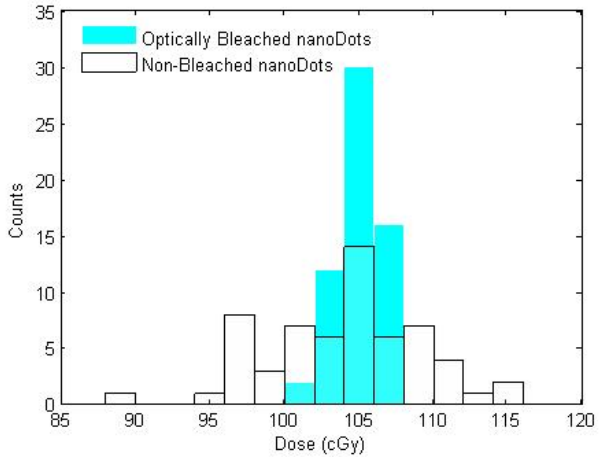

Figure 4.8: The absolute dose distribution histogram shows a more centrally peaked distribution for optical bleached nanoDot™ dosimeters compared to non-optically bleached dosimeters for 20 iterations of 100 cGy. The each data set consists of 20 measurements of dose for three dosimeters. The histogram dose bins are 2 cGy.

is less than ideal because of the higher accumulative dose points in our data set that would suggest that a polynomial of greater degree is a better fit. Both fits only help to understand the general behavior of the reproducibility of the nanoDot™ dosimeters and do not provide absolute predictive behavior for the device that would be necessary for clinical application.

The histogram of the data sets, shown in Fig.(4.8), illustrates the wide distribution of absolute dose measurements for the accumulative dose method of repeat use compared to the optical bleaching method of repeated use. Although the dose is comparatively more centrally peaked for the optical bleaching data set, the peak is centered at 105 cGy demonstrating precision but lack of accuracy for 6 MV repeat irradiations.

Normalizing the optically bleached data either by the first dose reading or the average of the first three readings would shift the entire data set so the peak is at 100 cGy.

This in turn would suggest this method of optical bleaching would be a viable way to reuse these dosimeters. However, in the clinic when a dosimeter is used, a normalizing or correction factor is not necessarily known. Ideally, a new calibration curve would be available to convert the dosimeter reading to the correct.

The uncertainty of in each measurement is also a source of difference between the two data sets. The uncertainty of the optically bleached dosimeters remains quite low where the non-bleached dosimeters have an increase uncertainty in measurement. The uncertainties in each measurement for the two data sets are shown in Fig.(4.9). For the entire experiment, the bleached nanoDot™ dosimeters uncertainty remains below 2%. The uncertainty of the non-bleached dosimeters increases with every measurement except for a few cases and eventually reaches a maximum of 12.4%.

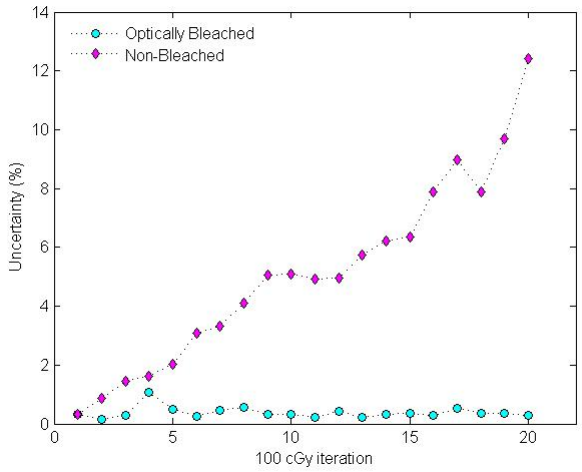

Figure 4.9: The uncertainty for the non-bleached dosimeters rises over the course of the entire experiment while the uncertainty for the bleached dosimeters remains below 2% for dosimeters irradiated with a 6 MV photon beam.

As a clinical tool, a dosimeter with uncertainty above 5% would have limited uses.

The nanoDot™ dosimeters are sold as a device with 3% or less uncertainty. Allowing 3% uncertainty to serve as a benchmark, optically bleaching nanoDot™ dosimeters prior to use can extend the usage of a dosimeter. And, if a dosimeter is repeatedly used without bleaching, the uncertainty becomes too large to trust the measurement after 5 uses.

The absolute dose data for repeat measurement experiment with a 10 MV photon beam is shown in Fig.(4.10). The uncertainty for each of the measurements is plotted alone in Fig.(4.11) and a histogram of the absolute dose is shown in Fig.(4.12).

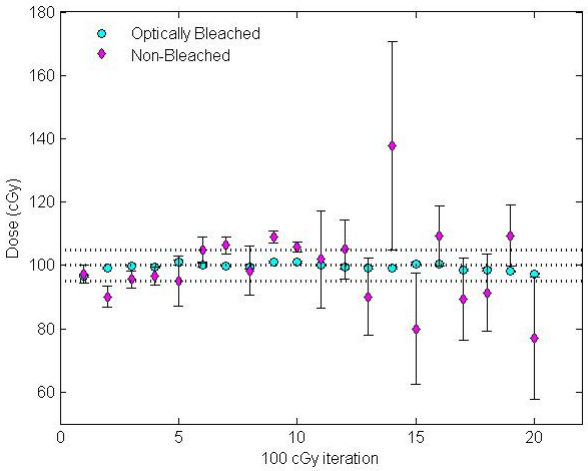

Figure 4.10: The absolute dose reading for optical bleached nanoDot™ dosimeters and non-optically bleached dosimeters for 20 iterations of 100 cGy for a 10 MV photon beam. Dashed lines represent 95, 100, and 105 cGy.

The uncertainty of the bleached is better than the uncertainty of the non-bleached dosimeters in the 10 MV repeated irradiation experiment. The maximum uncertainty value of the bleached dosimeters is 0.75 %, while the non-bleached dosimeters eventually reach an uncertainty value of 32.97 %.

The absolute dose of the bleached dosimeters in our experiment has less variability

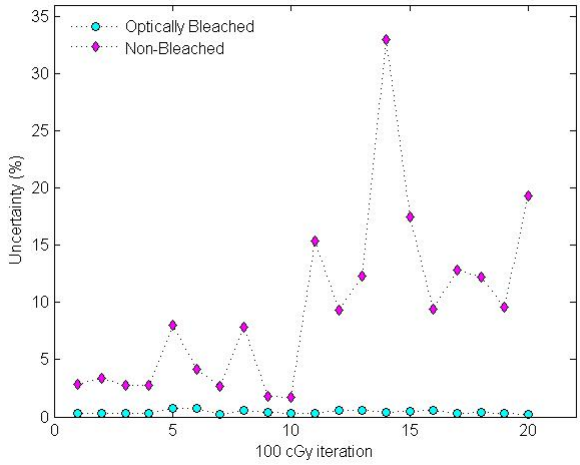

Figure 4.11: The uncertainty for the non-bleached dosimeters rises over the course of the entire experiment while the uncertainty for the bleached dosimeters remains below 2% for dosimeters irradiated with a 10 MV photon beam.

when compared to the absolute dose of the non-bleached dosimeters. The minimum and maximum dose for the bleached dosimeters is 94.89 cGy and 103.18 cGy, respectively. The bleached dosimeters also have a mean value of 99.48 cGy with a standard deviation of 2.16 cGy. The non-bleached dosimeters have a minimum and maximum value of 54.98 cGy and 173.83 cGy, respectively. The data set has a mean value of 99.55 cGy with a standard deviation of 16.15 cGy.

The repeated measurement experiment for nanoDot™ dosimeters irradiated with an 18 MV photon beam are shown in Fig.(4.13). The uncertainty for each of the measurements is plotted in Fig.(4.14) and a histogram of the absolute dose in Fig.(4.15). The uncertainty for the bleached dosimeter remains less than 2% for all measurements while the uncertainty for the non-bleached dosimeters increases with every measurement and has a maximum value of 13.8%. The histogram of the absolute dose shows the varia-

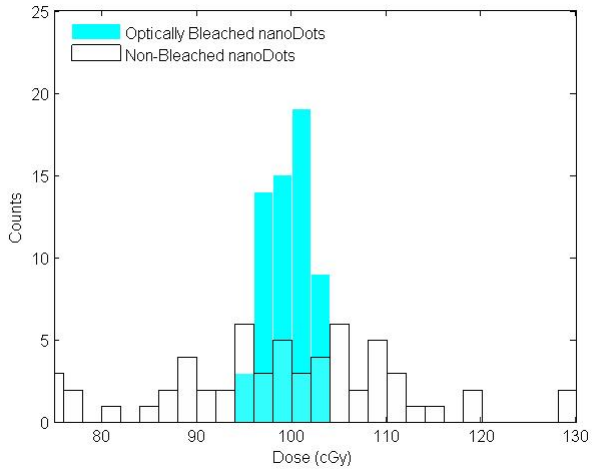

Figure 4.12: The absolute dose distribution histogram for 10 MV repeat irradiations shows a more centrally peaked distribution for optical bleached nanoDot™ dosimeters with a mean value of 99.48 cGy and a standard deviation of 2.162 cGy compared to non-optically bleached dosimeters for 20 iterations of 100 cGy. The each data set consists of 20 measurements of dose for three dosimeters. The histogram dose bins are 2 cGy.

tion in measurements for the non-bleached dosimeters with a maximum value of 142.49 cGy and a minimum value of 69.22 cGy. The average reading is 98.94 cGy with a standard deviation of 10.85 cGy. The optically bleached dosimeters, in contrast, have a very centrally peaked distribution with a minimum and maximum value of 95.95 cGy and 103.19 cGy, respectively. The mean value for the bleached dosimeters is 99.81 cGy with a standard deviation of 1.59 cGy.

4.4 Low Dose Sensitivity Changes

The four linear calibration curves generated from pre-irradiated dosimeters that have been optically bleached are presented in Fig.(4.16). The plot of our data shows the differences in slopes of the curves. The more total dose the dosimeter was pre-irradiated

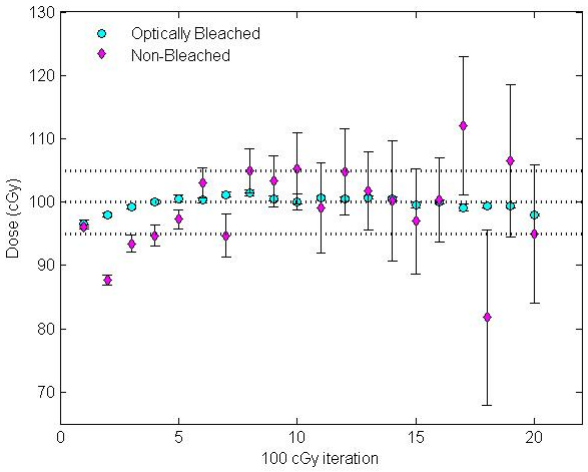

Figure 4.13: The absolute dose reading for optical bleached nanoDot™ dosimeters and non-optically bleached dosimeters for 20 iterations of 100 cGy for a 18 MV photon beam. Dashed lines represent 95, 100, and 105 cGy.

with, the less its slope on a plot of counts per dose.

The four linear calibration curves are compared to each other statistically using the procedure outline in the method section. The null hypothesis states that the two curves being compared are the same and do not require a coupling term while the alternative hypothesis states the curves are different and would require a coupling term to describe the two data sets as one. The results are shown in Table(4.3) along with the associated p-value. In every case except when comparing the calibration curves generated from pre-irradiated dosimeters with 10 and 20 Gy, there is strong evidence against the null hypothesis. Thus, in all instances except the one, the data sets are different enough to constitute their own linear curve.

Our results in the linear dose range of the dosimeters shows that the sensitivity increases with accumulative dose after optical bleaching. Thus, fewer counts will register

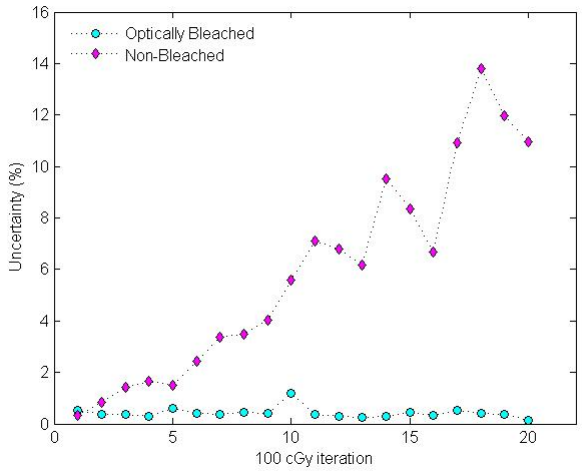

Figure 4.14: The uncertainty for the non-bleached dosimeters rises over the course of the entire experiment while the uncertainty for the bleached dosimeters remains below 2% for dosimeters irradiated with a 18 MV photon beam.

as a higher dose when reading out the device as the device accumulates dose. This is contradictory to previous published results which looked at sensitivity changes with accumulative dose for these dosimeters (Jursinic, 2010).

A couple of reasons exist that can account for the differences in sensitivity predictions of the OSL dosimeters with accumulating dose. Firstly, the published results look at the large scale behavior focusing on the large differences in dosimeter with accumulative dose seen in the non-linear region. Thus, the supra-linearity is reported as increasing equating to a decrease in sensitivity. Our experiment only focuses on the linear region dose response with accumulating dose, which could be considered very minute when compared to the supra-linearity changes. Secondly, the published results fit the dose response of the dosimeters to a single function. Thus, the variation at low doses may be within the variation of their fit. We feel there is a discontinuity between the linear and

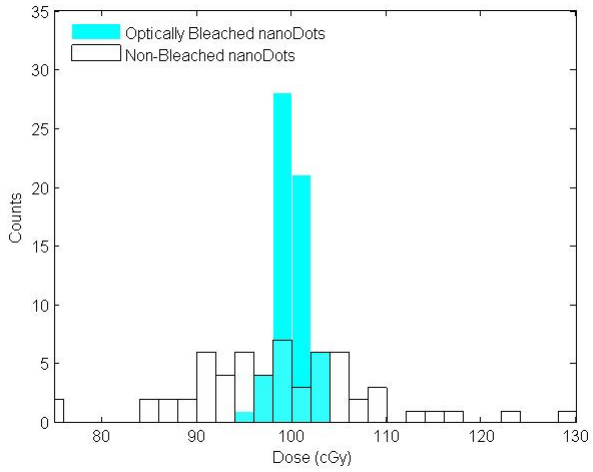

Figure 4.15: The absolute dose distribution histogram for 18 MV photon repeat irradiations shows a more centrally peaked distribution for optical bleached nanoDot™ dosimeters with a mean value of 99.81 cGy and a standard deviation of 1.59 cGy compared to non-optically bleached dosimeters for 20 iterations of 100 cGy. The each data set consists of 20 measurements of dose for three dosimeters. The histogram dose bins are 2 cGy.

non-linear region and each region should be analyzed separately.

Our goal for performing this experiment is to provide evidence that new calibration curves generated with OSL dosimeters with accumulative dose could be used for dosimeters that have accumulative dose and optically bleached. However, the increase in sensitivity that our data shows for these dosimeters with increase accumulative dose does not explain the high dose measurements from our repeatability experiments. If the new calibration curves are used to determine the dose in the repeatability experiment, the reported dose would rise further increasing the inaccuracy.

The method in which the calibration curves are generated may add to explanation to why they cannot be used to determine the dose accurately in the repeatability experiment. The new curves are generated with the method of allowing the dose accumulated

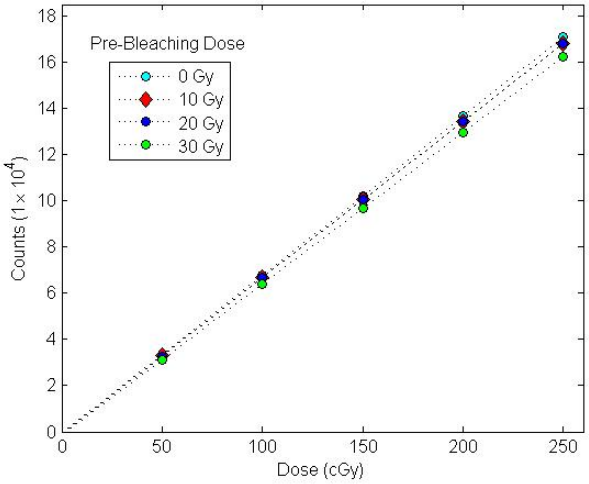

Figure 4.16: In the linear region of dose response for the OSL dosimeters, the dosimeters become more sensitive with accumulative dose.

Table 4.3: Linear Curve Comparison Results

Curves Compared	p-value
0 to 10	0.021
0 to 20	0.034
0 to 30	0.0002
10 to 20	0.951
10 to 30	0.0067
20 to 30	0.0085

on the dosimeter while determining the calibration curve. In comparison, the repeatability method uses a calibration curve based on the single use method for generating the dose points for a calibration curve.

The sensitivity experiment is continued for more than twenty 100 cGy iterations and shown in Fig.(4.17). The first 20 iterations show a slight increase at 10 Gy but a large fall off after 20 Gy. It has been reported by Jursinic in 2007 that the fall off in counts

is 4% per 10 Gy after 20 Gy of accumulative dose. As our data show the fall off in counts is not constant but plateaus around 60 Gy and actually begins to rise after 80 Gy. Eventually, the counts per 100 cGy irradiation are higher than for a new dosimeter.

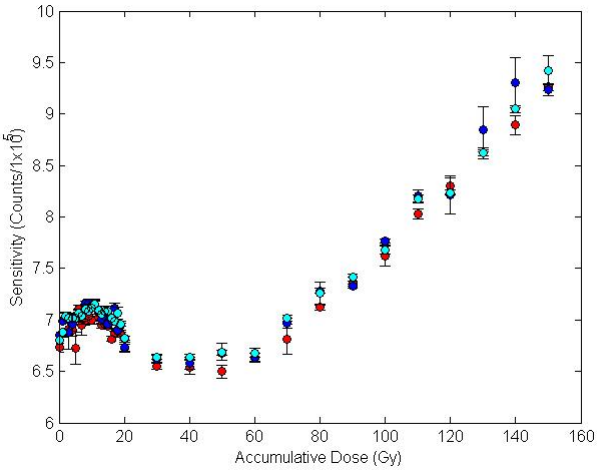

Figure 4.17: The recorded counts per 100 cGy of irradiation for three separate nanoDot™ dosimeter changes with accumulative dose. Each of the dosimeters is bleached for 20 minutes after irradiation and read out.

The change in sensitivity suggests an inter play between traps that are changed with accumulative dose. An increase of counts per 100 cGy irradiation at high accumulative dose could be due to a large amount deep traps being filled compared to when the dosimeter had less accumulative dose. This would lead to more intermediate traps being filled because of a lack of availability of deep traps. Thus, the read out would register more counts.

The decrease in counts per 100 cGy irradiations suggests more complexity in the interplay of traps. To register less counts either more electrons have to decrease their preference in intermediate traps or less intermediate traps must exists for read out. It is

unlikely that the statistical preference of the electron would change due to accumulative dose. However, if the fill of some deep traps cause a slight change in the local electric fill, some intermediate traps could be affected in such a way to strengthen their hold on an electron. Therefore, these coupled intermediate traps would not be available for stimulation and would not contribute to the amount of counts during read out.

It should be stated that our observations could be explained by the complex interplay between traps with accumulative dose, but our experiment does not explicitly demonstrate such speculation. We are offering an attempted explanation of interesting data.

4.5 INTRABEAM™ Application

4.5.1 Ion Chamber Quality Assurance

The first of our experiments use the nanoDot™ dosimeters with the 25% fill stage. The average corrected counts per dose rate is 284561 with 1σ uncertainty of 4907, approximately a 1.72% uncertainty in counts. To analyze how sensitive this method is, an analysis is performed which introduces error and looks for positive detection.

We introduce error by increasing the dose rate to simulate a failing ion chamber. A comparison can be made with the correct average counts per dose rate and then a recalculation of the average counts per dose rate given the new erroneous dose rate. The bounds of the measurements as determined by the uncertainty can be compared to find the percent error in the system that would be outside the range of where the uncertainties in the two measurements do not overlap. A 3.6% error in an ion chamber measurement

would be detectable by the current method as shown in Table(4.4).

Table 4.4: Ion Chamber Quality Assurance Test Results for 50 kVp Output

Data Set	Dose Rate (Gy/min)	Counts/Dose (Counts/Gy)	1-σ Range For Counts/Dose	Error Detected?
Correct Reading	2.513	284561	[279654, 289469]	
3.5% Error	2.601	274939	[270197, 279681]	No
3.6% Error	2.603	274723	[269985, 279461]	Yes
10% Error	2.764	258693	[254231, 263154]	Yes

The effect the stage has on dose reading is seen when a comparison is made between a stage of 35% fill is used instead of the 25% fill. The average counts per dose rate is 291715 with a 1σ uncertainty of 6240 counts, approximately 2.14%. An increase of 2.5% in actual counts per dose rate is seen along with a 27.1% increase in uncertainty.

The differences seen when comparing the 35% fill stage results to the 25% fill are not unexpected. The difference in fill will cause a variation in the amount of backscatter from the stage back into the dosimeter. The higher fill equates to a higher density of material giving the x-rays more opportunity to scatter.

The next experiments use the nanoDot™ dosimeters with the 25% fill stage with the INTRABEAM™ irradiating with 40 kVp beam. The average corrected counts per dose rate is 287182 with 1σ uncertainty of 6456, approximately a 2.24% uncertainty in counts. Again, we introduce error by adjusting the dose rate value and finding at what percent error produces counts per dose rate outside of the uncertainty for the correct reading. An error of 4.6% or greater is detectable by this method.

The counts per dose rate for the 40 kVp are less than 1% different than the counts per dose rate for the 50 kVp. However, the uncertainty for the 40 kVp is greater than for

Table 4.5: Ion Chamber Quality Assurance Test Results for 40 kVp Output

Data Set	Dose Rate (Gy/min)	Counts/Dose (Counts/Gy)	1-σ Range For Counts/Dose	Error Detected?
Correct Reading	1.506	287182	[280726, 293638]	
4.5% Error	1.574	274815	[268637, 280993]	No
4.6% Error	1.575	274553	[268380, 280725]	Yes
10% Error	1.657	261075	[255205, 266944]	Yes

the 50 kVp resulting in less sensitivity for the detection capabilities.

4.5.2 Distance Measurements

The dose for the measurements made at a distance for the ion chamber and the nanoDot dosimeters are shown in Table(4.6). The high degree of error at the 0.2 cm measurement point is most likely related to an experimental setup difference between the placement of the ion chamber and the dosimeter. The high dose gradient makes positioning an essential part of the setup to limit the amount of difference between the two measurements.

Table 4.6: Dose Measurements from Ion Chamber and nanoDot™ Dosimeters

Distance (cm)	Ion Chamber Dose (cGy)	Dosimeter Dose (cGy)	Error (%)
0.2	239.82	247.04	9.95
0.5	155.67	145.94	9.95
0.7	108.23	97.233	9.95

Given the limited data, the best fit to the data is an exponentially decreasing function. The fit of the ionization chamber data set is $Dose = 500e^{-2.35*Distance}$, while the fit for the dosimeter data set is $Dose = 500e^{-2.44*Distance}$. A quadratic equation could also fit

both data sets, but this fit seemed unlikely because of the positive quadratic term, which means the dose would increase at large distances when the dose is expected to reach zero as the distance increases.

It should be noted that the solid water used in this experiment is intended for beams in the megavoltage range. Although this was understood at the time of design the resources were not available to conduct an experiment with solid water that is designed for low keV irradiations. However, it is our intent to establish a general trend in the behavior of the dose at this range and provide a point for comparison for future experiments with solid water designed for low keV irradiations.

4.5.3 Patient Dose Measurements

Our knowledge of the dose response of the nanoDot™ dosimeters allows us to determine the dose to the skin for patients receiving the intraoperative procedure. The skin dose of patients as determined from the nanoDot™ dosimeters are listed in Table(4.7) along with the maximum dose.

Table 4.7: Patient Dose Measurements

Patient	Orange (cGy)	Black (cGy)	Purple (cGy)	Cyan (cGy)	Max Dose (cGy)
1	40.4	284.6	571.6	55.5	571.6
2	242.1	221.7	264.7	193.5	264.7
3	285.0	451.4	506.9	362.0	506.9
4	86.7	179.9	284.0	154.2	284.0
5	320.1	222.5	488.7	441.2	488.7

The dose readings are dependent on the placement of the dosimeters on the patient

relative to the INTRABEAM™ applicator. Also, the dose is dependent on the applicators relative position to the surface of the patient. However, the maximum skin dose is the most important detail when correlating the skin dose to skin toxicity.

Correlating the skin dose to skin toxicity gives two distinct possibility of improving patient treatment. First, follow up care can be correctly anticipated and allow health care providers information to properly prepare the patient for skin effects or skin reactions. Secondly, now that the skin dose can be measured directly it can be use to confirm the calculated dose to the skin with treatment planning software. This will open up the possibility of further defining criteria, such as tumor to surface distance, for patient treatment.

5 Conclusions

5.1 Initial Experiments

The simplicity of the initial set of experiments leads one to conclude that given the setup we are using the method of reading out the dosimeters is correct. The general trend of the the dose depletion and the dose response experiments are in agreement with published results. The variation seen the dose response experiment though does suggest the possibility that a high variability exists between batches of dosimeters. Considering batches contain 50 dosimeters is hard to image new calibration curves being created for every batch given that a calibration curve could use up to 30 dosimeters.

5.2 Conclusion of Optical Bleaching

Compared to other methods of optically bleaching nanoDot™ dosimeters, our method of using a light box can effectively reduce the dose on the dosimeters after 1 hour by 99% its original dose. As compared to other methods already discussed, this method is neither the best nor the worst method for bleaching. However, the method is effective and uses equipment that is found in most clinics. It would not be hard to start bleaching the dosimeters with nothing more than dedicated space and time.

The percentage of remaining dose is a useful measure of the efficiency of the bleaching method but the absolute dose remaining on the dosimeter is more important for re-

peated use in the clinic. To reduce the accumulative dose to those comparable to new dosimeters, $dose \approx 0.02cGy$, multiple days of bleaching should be employed depending on the dose on the dosimeter.

5.3 Repeatability

The main question we're trying to answer with our repeatability experiments is what is the most accurate way to reuse nanoDot™ dosimeters. Unfortunately, the three different energy photon beams we used to compare repeatability measurements between bleach and non-bleached nanoDot™ dosimeters tell different stories.

The similarities between all three irradiating energies is the low standard deviation seen for bleached nanoDot™ dosimeters and the increasing uncertainty in measurements for non-bleached dosimeters. The extreme difference between measurements after five or more irradiations paints a positive picture for the bleaching method for reusing the dosimeters. Using the criteria that an uncertainty of greater than 5% would not be useful as a measurement tool, the bleached dosimeters could be used 20 times while the non-bleached dosimeters would not be useful after 5 irradiations. The uncertainty shows the precision of the bleached dosimeters is very high and consistent for the duration of our experiment.

The reported absolute dose for the non-bleached nanoDot™ dosimeters also show a similar behavior across 6, 10, and 18 MV photon energies. Even though the mean of the measurements is close to 100 cGy, the high standard deviation is evident of the high variability in the measurements. Therefore, across all energies allowing the dose to

accumulate on the dosimeter leads to a low amount of accuracy in dose measurements when repeatedly used.

A difference can be seen when comparing the absolute dose for bleached nanoDot™ dosimeters across all three energies. All three show a relatively low deviation from the central peak, but the placement of the central peak is the difference. The 6 MV dose distribution is centered around 105 cGy, while the 10 and 18 MV energies are centered at 99.48 and 99.81 cGy, respectively. If the uncertainty is a measure of precision and the mean is a measure of the accuracy, the 6 MV dose distribution is precise but not accurate and the 10 MV distribution is accurate but the least precise. The 18 MV dose distribution is both accurate with a mean of 99.81 cGy and precise with a standard deviation of 1.59 cGy.

The outcomes of our repeatability experiment suggest at higher energies the ability to reuse nanoDot™ dosimeters becomes more plausible without the need for further calibrations. At 6 MV, a new calibration curve is needed to account for the lack of accuracy and reusing nanoDot™ dosimeters with 10 MV may not be possible due to the variability.

If the reuse of the nanoDot™ dosimeter is sought after, our data shows reuse without optically bleaching the dosimeter leads to a reported dose that is neither accurate or precise. Simply subtracting the final dose from the initial dose for a single irradiation produced the most variation and uncertainty in our experiment.

The sensitivity changes seen in the nanoDot™ dosimeters beyond 20 Gy leads to some interesting conclusions. Of course, the speculation of the interplay between deep traps is interesting and should be investigated further, but may require specialized equip-

ment beyond the scope of clinical machinery. However, if investigations could show that the sensitivity changes in a predictable way, dosimeters with accumulative dose may become manageable throughout a large dose range.

In contrast, the search for other sensitivity plateau regions should continue which may identify regions of low sensitivity changes that could be exploited for dosimetric purposes. In this scenario, the dosimeters are only useful in plateau regions of accumulative dose ranges. Our data shows another possible region of low sensitivity change may exist for accumulative doses of 50 to 80 Gy. This may point to a use case where once a dosimeter has close to 20 Gy, it is irradiated for an amount of dose so the accumulative dose reaches 50 Gy. Then, for 30 Gy more the nanoDot™ dosimeter will be useful again with a new calibration curve. If other plateau regions are found, the dosimeter would continue to be dosed up to subsequent regions.

5.4 INTRABEAM™ Application

5.4.1 Ion Chamber Quality Assurance

The nanoDot™ dosimeters can ensure the functionality of the ion chamber by detecting a variation in the reported dose rate. Since the ion chamber does not have its own quality assurance procedure, the length of treatment would be incorrect if the dose rate is misreported to the system. Without a procedure in place to check the ion chamber reading, it is unlikely an error will be detected prior to treatment. An error might not be detected until the ion chamber is sent out for recalibration which is scheduled for every

two years.

Our procedure for the quality assurance for the ion chamber using nanoDot™ can serve as an easy quick first step in the detection of a malfunction of the ion chamber. If our method detects a fail, a more in depth inquiry should commence using known x-ray sources with established dose rates to further determine the functionality of the ion chamber.

It should also be noted that our test is dependent on the consistent usage of the mounting stage. Our experiments with a different fill percentage resulted in a significant change in the counts per dose rate constant. The two fill percentages only differ by 10% and a 2.5% difference is detected in the derived constant, which leads to a 1% difference in error detection ability. Even though there is an overlap in the range of a 1σ deviation from the mean, the actual mean counts per dose rate from the two different fills would be detected as an error by the other.

5.4.2 Distance Measurements

The general trend of an exponentially decreasing dose with distance is seen with our experiment whether the ion chamber or nanoDot™ dosimeters are used to measure the dose. However, the high dependence on the positioning of the measurement devices and the fact that the materials used in the setup are not designed for low keV irradiations stops us from making a definitive conclusion.

Our experiment does form a baseline for future experiments and it shows a dose fall off greater than at a linear rate. This fast fall off rate is promising and points to the

likelihood that the dose to the skin during treatment will remain low. Also, an error of less than 10% for all measurements shows promise for the future experiment when keV solid water is used.

5.4.3 Patient Data

We were able to determine the dose nanoDot™ dosimeter received while on the skin of patient receiving INTRABEAM™ treatment. What is believed to be the largest source of error is the incident angle of radiation due to the orientation of the nanoDot™ dosimeters which is unknown. Although measures can be taken during the placement of the dosimeters to ensure they are flat against the body, contours of the body prevent the normal of the dosimeter to be radial parallel to the applicator. In studies with mammography, the reduction of dose is approximately 10% at 45^{circ} but increases rapidly to 80% deduction at 90^{circ}

6 Future Considerations

6.1 Ion Chamber Quality Assurance

Although there are many other applications that the nanoDot™ dosimeter could be used for, there are a few interesting improvements that could be made on our method of quality assurance for ion chambers used with the INTRABEAM™ system.

First of all, using an external live source to provide the electrometer in the system with the minimum current is trouble some. The live source requires extra safety precautions that come with transporting and handling live sources. A serious improvement to the procedure could be made if the live sources were not used. The electrometer needs to run in an output mode of 300 volts. A simple circuit could be designed to give the electrometer the necessary current using this voltage source.

Secondly, it would be nice to know the variability in construction with the 3-D printer, namely, the variation in density for a given setting. This could effect the measurements due to backscatter and therefore not allow comparison of data over the entire use of the method.

Finally, experiments with different stage fill amounts could be performed to see the effect due to a change in density of the stage. Knowing how the effect of changing the fill setting during construction and know the variability in the construction at every fill setting will complete the picture for how to design the proper stage and give a better

measure of uncertainty in this method.

6.2 Customizable Phantoms

The construction of the nanoDot™ dosimeter stage with a 3-D printer opens up the possibility of customizable phantoms. The potential and the practicality of customizable phantoms should be explored for its use with medical dosimeter. The idea of using different types of plastics and varying the density could have an wide range of application from experimenting to quality assurance testing.

6.3 Measuring Points along the INTRABEAM™ Depth Dose Curve

The goal of this project is to allow users of the INTRABEAM™ system to measure their two or three points along the manufacturer supplied depth dose curve using nanoDot™ dosimeters. The idea is to correlate the nanoDot™ dosimeter measurements from the XRS probe to actual measurements performed in water by the same probe with the same output settings. The ability to measure these points independently allows the user to check the output of the XRS against the manufacturer supplied data, which is currently not possible in any capacity. A procedure based around this project could become part of the an annual or bi-annual quality assurance check for the device.

This project has significant challenges ranging from cross calibrating water chamber measurements to ion chamber measurements to nanoDot™ measurements all at the same depth; set-up and characterizing any materials that are used to hold any of chambers

in place; and characterizing angular dependent correction factors for orientation issues with the nanoDot™ dosimeters. Plus, some of the measurements will be done in water and the supplied ion chamber is not water proof.

6.4 INTRABEAM, Xoft, and External Beam Radiation

Our experiments are helping to understand the correct way to interpret results for nanoDot™ dosimeters at the 50 keV range. Further experiments are need to achieve the optimal technique for using the dosimeters to measure skin dose to aid in treatment planning and assessment of delivery.

If emerging technologies hope to gain ground in the usage of treatment methods, a comparison study has to be done between the new technology and the current methods, namely external beam radiation therapy. NanoDot™ dosimeters can provide surface radiation details that are not currently directly measured. These types of measurements can provide information that can help determine the best type of treatment for a patient.

INTRABEAM™and Xoft are two new emerging technologies that deliver radiation using low keV x-rays, which are known to have a sharp drop off of dose in tissue. This sharp drop off could be looked at as an advantage over external beam radiotherapy(EBRT) because it reduces side effects primarily due to effects from skin radiation exposure. Thus, measuring the skin toxicity from these devices while being used in intraoperative radiation therapy is a high priority in order to compare effects to those of EBRT.

6.5 Eye Plaque

Eye plaque therapies use ^{125}I as a source for delivering dose to a patient's eye. As a source, ^{125}I emits a gamma at 35 keV. A project designed to measure patient surface dose with OSLDs would require characterization that includes this energy.

6.6 Real Time Dosimetry

Real time dosimetry with OSLDs is an emerging technology. Since nanoDot™ dosimeters stimulate with one wavelength and emit with another, the technology is moving quickly toward the possibility of real time dosimetry with a continuous stimulating light verses the pulsed light used for read out purposes. Investigations into this area of research could really open up options in the area of personal dosimeters by replacing passive dosimeters.

Bibliography

[1] M. Akselrod, N. Agersnap Larsen, V. Whitley, and S. McKeever. Thermal quenching of f-center luminescence in Al_2O_3:C. *J. Appl. Phys.*, 84(6):3364–3373, 1998.

[2] M. Akselrod and V. Kortov. Thermoluminescent and exoemission properties of new high-sensitivity tld α-Al_2O_3:C single crystal detectors. *Radiation Protection Dosimetry*, 33:123–126, 1990.

[3] M. S. Akselrod, V. Kortov, and E. Goreleva. Preparation and properties of α-Al_2O_3:C. *Radiat. Prot. Dosim.*, 47:159–164, 1993.

[4] M. S. Akselrod, V. S. Kortov, D. Krvetshky, and V. Gotlib. High sensitivity thermoluminescent anion-defective α-Al_2O_3:C crystal detectors. *Radiat. Prot. Dosim.*, 32:15–20, 1990.

[5] R. M. Al-Senan and M. R. Hatab. Characteristics of an OSLD in the diagnostic energy range. *Med. Phys.*, 38(7):4396–4405, 2011.

[6] P. R. Almond, P. J. Biggs, B. M. Coursey, W. F. Hanson, M. S. Huq, R. Nath, and D. W. Rogers. AAPM's TG-51 protocol for clinical reference dosimetry of high-energy photon and electron beams. *Med. Phys.*, 26(9):1847–70, Sept. 1999.

[7] K. S. Armoogum, J. M. Parry, S. K. Souliman, D. G. Sutton, and C. D. Mackay.

Functional intercomparison of intraoperative radiotherapy equipment - photon radiosurgery system. *Radiation Oncology*, 2(11), 2007.

[8] F. H. Attix. *Introduction to Radiological Physics and Radiation Dosimetry*, pages 395–437. John Wiley & Sons, Inc., New York, 1986.

[9] H. Bartelink, J.-C. Horiot, P. Poortmans, H. Struikmans, W. van den Bogaert, I. Barillot, A. Fourquet, J. Borger, J. Jager, W. Hoogenraad, L. Collette, and M. Pierart. Recurrence Rates after Treatment of Breast Cancer with Standard Radiotherapy With or Without Additional Radiation. *N Engl J Med*, 345(19):1378–1387, 2001.

[10] P. J. Biggs. Long-term stability of a 50-kv x-ray unit for stereotactic irradiation. *Journal of Applied Clinical Medical Physics*, 7(3), 2006.

[11] L. Bøtter-Jensen, S. W. S. McKeever, and A. Wintle. *Optically Stimulated Luminescence Dosimetry*. Elsvier, Amsterdam, 2003.

[12] B. Fisher, S. Anderson, J. Bryant, R. G. Margolese, M. Deutsch, E. R. Fisher, J.-H. Jeong, and N. Wolmark. Twenty-Year Follow-Up of a Randomized Trial Comparing Total Mastectomy, Lumpectomy, and Lumpectomy Plus Irradiation for the Treatment of Invasive Breast Cancer. *N Engl J Med*, 347(16):1233–1241, 2010.

[13] E. B. C. T. C. Group. Effect of radiotherapy after breast-conserving surgery on 10-year recurrence and 15-year breast cancer death: meta-analysis of individual patient data for 10 801 women in 17 randomised trials. *Lancet*, 378:1707–1716, Oct. 2011.

[14] P. A. Jursinic. Characterization of optically stimulated luminescent dosimeters, OSLDs, for clinical dosimetric measurements. *Med. Phys.*, 34(12):4594, 2007.

[15] P. A. Jursinic. Changes in optically stimulated luminescent dosimeter (OSLD) dosimetric characteristics with accumulated dose. *Med. Phys.*, 37(1):132, 2010.

[16] S. L. Kakani and A. Kakani. *Material Science*. New Age International Publishers, 1^{st} edition, 2004.

[17] Kaye & Laby Table of Physical & Chemical Constants. 2012. National Physical Laboratory. 18 Nov. 2012 *//www.kayelaby.npl.co.uk/atomic_and_nuclear_physics/4_2/4_2_1.html*.

[18] J. R. Kerns, S. F. Kry, N. Sahoo, D. S. Followill, and G. S. Ibbott. Angular dependence of the nanodot osl dosimeter. *Med. Phys.*, 38(7):3955–3962, July 2011.

[19] F. M. Khan. *The Physics of Radiation Therapy*. Lippincott Williams & Wilkins, 4^{th} edition, 2010.

[20] T. H. Kirby and D. A. Hanson, W. F. and. Johnston. Uncertainty analysis of absorbed dose calculations from thermoluminescence dosimeters. *Med Phys*, 19(6):1427–1433, 1992.

[21] T. H. Kirby, W. F. Hanson, R. J. Gastorf, C. H. Chu, and R. J. Shalek. Mailable tld system for photon and electron therapy beams. *Int J Radiat Oncol Biol Phys*, 12(2):261–265, 1986.

[22] G. Knoll. *Radiation Detection and Measurment*. John Wiley & Sons, Inc., 4^{th} edition, 2010.

[23] U. Kraus-Tiefenbacher, A. Scheda, V. Steil, B. Hermann, T. Kehrer, L. Bauer, F. Melchert, and F. Wenz. Intraoperative radiotherapy (IORT) for breast cancer using the Intrabeam system. *Tumori*, 91(4):339–45, 2005.

[24] B. G. Markey, L. E. Colyott, and S. W. S. McKeever. Time-resolved optically stimulated luminescence from α- Al_2O_3:C. *Radiat. Meas.*, 24:457–463, 1995.

[25] S. McKeever. *Thermoluminescence of Solids*. Cambridge University Press, 1985.

[26] A. A. Omotayo, J. E. Cygler, and G. O. Sawakuchi. The effect of different bleaching wavelength on sensitivity of Al_2O_3:C optically stimulated luminescence detectors (oslds) exposed to 6mv photon beams. *Am. Assoc. Phys. Med.*, 39(9):5457–5468, September 2012.

[27] L. Pauling and S. B. Hendricks. The crystal structures of hermatite and corundum. *Journal of the American Chemical Society*, 47:781–790, 1925.

[28] C. Polgár, J. Fodor, Z. Orosz, T. Major, Z. Takácsi-Nagy, L. C. Mangel, Z. Sulyok, A. Somogyi, M. Kásler, and G. Németh. Electron and high-dose-rate brachytherapy boost in the conservative treatment of stage I-II breast cancer first results of the randomized Budapest boost trial. *Strahlentherapie und Onkol*, 178(11):615–23, Nov. 2002.

[29] P. Romestaing, Y. Lehingue, C. Carrie, R. Coquard, X. Montbarbon, J. M. Ardiet, N. Mamelle, and J. P. Gérard. Role of a 10-Gy boost in the conservative treatment

of early breast cancer: results of a randomized clinical trial in Lyon, France. *J Clin Oncol*, 15(3):963–8, Mar. 1997.

[30] J. K. Shultis and R. Faw. *Fundamentals of Nuclear Science and Engineering*. Marcel Dekker, Inc., 2002.

[31] B. D. Smith, D. W. Arthur, T. a. Buchholz, B. G. Haffty, C. a. Hahn, P. H. Hardenbergh, T. B. Julian, L. B. Marks, D. a. Todor, F. a. Vicini, T. J. Whelan, J. White, J. Y. Wo, and J. R. Harris. Accelerated partial breast irradiation consensus statement from the American Society for Radiation Oncology (ASTRO). *Int. J. Radiation Oncology Biol. Phys.*, 74(4):987–1001, July 2009.

[32] N. Tsoulfanidis. *Measurement and Detection of Radiation*. Taylor & Francis, Washington, DC, 2^{nd} edition, 1995.

[33] J. E. Turner. *Atoms, Radiation, and Radiation Protection*. Wiley-VCH Verlag GmbH & Co. KGaA, Weinheim, 3^{rd} edition, 2007.

[34] J. S. Vaidya, D. J. Joseph, J. S. Tobias, M. Bulsara, F. Wenz, C. Saunders, M. Alvarado, H. L. Flyger, S. Massarut, W. Eiermann, M. Keshtgar, J. Dewar, U. Kraus-Tiefenbacher, M. Sütterlin, L. Esserman, H. M. R. Holtveg, M. Roncadin, S. Pigorsch, M. Metaxas, M. Falzon, A. Matthews, T. Corica, N. R. Williams, and M. Baum. Targeted intraoperative radiotherapy versus whole breast radiotherapy for breast cancer (TARGIT-A trial): an international, prospective, randomised, non-inferiority phase 3 trial. *Lancet*, 376(9735):91–102, July 2010.

[35] J. A. van Dongen, A. C. Voogd, I. S. Fentiman, C. Legrand, R. J. Sylvester, D. Tong, E. van der Schueren, P. A. Helle, K. van Zijl, and H. Bartelink. Long-term results of a randomized trial comparing breast-conserving therapy with mastectomy: European Organization for Research and Treatment of Cancer 10801 trial]. *J Natl Cancer I*, 92(14):1134–1150, Apr. 2000.

[36] U. Veronesi, N. Cascinelli, L. Mariani, M. Greco, R. Saccozzi, A. Luini, M. Aguilar, and E. Marubini. Twenty-year follow-up of a randomized study comparing breast-conserving surgery with radical mastectomy for early breast cancer. *N Engl J Med*, 347(16):1227–32, Oct. 2002.

[37] F. Wenz, F. Schneider, C. Neumaier, U. Kraus-Tiefenbacher, T. Reis, R. Schmidt, and U. Obertacke. Kypho-IORT–a novel approach of intraoperative radiotherapy during kyphoplasty for vertebral metastases. *Radiation Oncology*, 5:11, Jan. 2010.

[38] E. Yukihara and S. McKeever. Optically stimulated luminescence (osl) dosimetry in medicine. *Physics in Medicine and Biology*, 53, 2008.

[39] E. G. Yukihara, V. H. Whitley, S. W. S. McKeever, A. E. Akselrod, and M. S. Akselrod. Effect of high-dose irradiation on the optically stimulated luminescence of Al_2O_3:C. *Radiat. Meas.*, 38, 2004.

[40] E. G. Yukihara, V. H. Whitley, J. C. Polf, D. M. Klein, S. W. S. McKeever, A. E. Akselrod, and M. S. Alselrod. The effect of deep trap population on the thermoluminescence of Al_2O_3:C. *Radiat. Meas.*, 37, 2003.